

January 2008

# Dynamic Reconfiguration Techniques for Wireless Sensor Networks

Cheng-tai Yeh

*University of Massachusetts Amherst*, [cych@ecs.umass.edu](mailto:cych@ecs.umass.edu)

Follow this and additional works at: <http://scholarworks.umass.edu/theses>

---

Yeh, Cheng-tai, "Dynamic Reconfiguration Techniques for Wireless Sensor Networks" (2008). *Masters Theses 1911 - February 2014*. 119.

<http://scholarworks.umass.edu/theses/119>

This thesis is brought to you for free and open access by the Dissertations and Theses at ScholarWorks@UMass Amherst. It has been accepted for inclusion in Masters Theses 1911 - February 2014 by an authorized administrator of ScholarWorks@UMass Amherst. For more information, please contact [scholarworks@library.umass.edu](mailto:scholarworks@library.umass.edu).

**DYNAMIC RECONFIGURATION TECHNIQUES FOR WIRELESS  
SENSOR NETWORKS**

A Thesis Presented

by

CHENG-TAI YEH

Submitted to the Graduate School of the  
University of Massachusetts Amherst in partial fulfillment  
of the requirements for the degree of

MASTER OF SCIENCE IN MECHANICAL ENGINEERING

May 2008

Mechanical and Industrial Engineering Department

© Copyright by Cheng-tai Yeh 2008

All Rights Reserved

**DYNAMIC RECONFIGURATION TECHNIQUES FOR WIRELESS SENSOR  
NETWORKS**

A Thesis Presented

by

CHENG-TAI YEH

Approved as to style and content by:

---

Robert X. Gao, Chair

---

Weibo Gong

---

Abhijit Deshmukh

---

Mario Rotea, Department Head  
Mechanical and Industrial Engineering  
Department

## ACKNOWLEDGEMENTS

I would like to express my appreciation to Professor Robert X. Gao, for his time, patience, and understanding through my M.S. study. His encouragement drove me to the successful completion of my research. Under his help, I have not only learned the essence of research, but also improved my way of thinking, analyzing, and presenting. I believe the training I received under his guidance will benefit all me life. Specially, I am very grateful for him to give me the opportunity to work on the exciting topic of wireless sensor network. I would also like to thank Professor Abhijit Deshmukh and Professor Weibo Gong for serving on my thesis committee and providing valuable feedbacks on my research.

My gratitude also goes to Electromechanical Systems Laboratory (EMSL). There are not enough words to describe your great work. Zhaoyan Fan, Raymond Frenkel, Dr. Abhijit Ganguli, M. Haris Hamid, Abhijit Kadrolkar, Shaopeng Liu, Sripati Sah, Ruqiang Yan, and Shuangwen Sheng - you were there to give me help no matter what time or day of the week it was. Special thanks to Ray - you always had time to help no matter how busy you were. Last but not least, I would like to acknowledge funding provided to my research by the National Science Foundation under grant DMI-0330161.

Lastly, I would like to express thanks to my family for their support during my stay in Amherst.

## **ABSTRACT**

### **DYNAMIC RECONFIGURATION TECHNIQUES FOR WIRELESS SENSOR NETWORKS**

MAY 2008

CHENG-TAI YEH, B.S., NATIONAL TAIWAN UNIVERSITY

M.S., UNIVERSITY OF MASSACHUSETTS AMHERST

Directed by: Professor Robert X. Gao

The need to achieve extended service life from battery powered Wireless Sensor Networks (WSNs) requires more than state-of-the-art low-power hardware designs based on fixed hardware platforms and energy-efficient protocols. Recent advancements in reconfigurable hardware designs that adapt a circuit's energy consumption to external dynamics motivated the present study. Dynamic Voltage Scaling (DVS), Dynamic Modulation Scaling (DMS), and recharge of sensor nodes allow the supply voltage and operating frequency of the CPU, the modulation level of the radio, and sensing activity of sensor nodes to be varied dynamically to reduce the energy consumed for computation and communication.

This thesis presents a framework for the utilization of reconfigurable techniques on a WSN at the node-level and at the network-level. For node-level reconfiguration, an integration of DVS and DMS techniques was proposed to minimize the total energy consumption. A dynamic time allocation algorithm was developed that utilized the special structure of the optimization problem and a classification of a sensor nodes' energy optimization function to efficiently solve the time allocation problem. The

simulation results demonstrated an average of 55% energy reduction. Furthermore, performance improvement of the DVS algorithm in high communication tasks and high node numbers was also demonstrated by combining the DMS with DVS.

For network-level reconfiguration, a node activation technique was presented to reduce the cost of recharging energy-depleted sensor nodes. Network operation combined with node activation was modeled as a stochastic decision process, where the activation decisions directly affected the energy efficiency of the network. An analytical model was developed to formulate the network operation as a Semi-Markov Decision Process by assuming exponentially distributed recharging and discharging times. Using this model, an optimal activation policy was obtained that minimized the recharging rate. The results of this work were simulated for a correlated sensor model with a 72% reduction of recharging rate. A reconfigurable sensor network based on the DVS concept was implemented that enabled continued data sampling and on-node data feature extraction. Energy reduction of up to 50% was achieved using the reconfigurable sensor hardware, which effectively translates into prolonged service life of the sensor network.

## TABLE OF CONTENTS

	Page
ACKNOWLEDGEMENTS .....	iv
ABSTRACT .....	v
LIST OF TABLES .....	ix
LIST OF FIGURES .....	x
1. INTRODUCTION .....	1
1.1 Wireless Sensor Networks .....	1
1.2 Energy-Efficient Techniques .....	4
1.3 Dynamic Reconfiguration .....	5
1.4 Motivation .....	6
2. PROBLEM STATEMENT .....	7
3. RESEARCH TASKS .....	8
3.1 Node-Level Reconfiguration .....	8
3.1.1 Literature Review .....	8
3.1.2 DVS Technique .....	10
3.1.3 DMS Technique .....	12
3.1.4 Dynamic Time Allocation .....	16
3.1.4.1 Single-Node Scenario .....	17
3.1.4.2 Multi-Node Scenario .....	21
3.1.4.3 Network Sectioning .....	21
3.1.4.4 Data Acquisition Scheme .....	22
3.1.4.5 Communication Protocol .....	23
3.1.4.6 Solution Formulation .....	25
3.1.4.7 Dynamic Time Allocation Algorithm .....	26
3.1.5 Simulation Model and Results .....	32
3.2 Network-Level Reconfiguration .....	38
3.2.1 Background .....	39
3.2.2 Literature Review .....	41
3.2.3 Semi-Markov Decision Process .....	46
3.2.3.1 Model Definition .....	47



3.2.3.2 Transition Properties.....	48
3.2.3.3 Solution Formulation .....	52
3.2.3.4 Value Iteration Algorithm.....	54
3.2.4 Simulation Model and Results .....	57
3.3 Implementation .....	61
3.3.1 Network Operation .....	62
3.3.1.1 Cluster Head Selection Algorithm.....	63
3.3.1.2 Time Synchronization Protocol .....	65
3.3.1.3 Dynamic Time Allocation.....	66
3.3.2 Sensor Node Design.....	67
3.3.3 Experiment.....	69
3.3.3.1 Experiment Setup.....	69
3.3.3.2 Energy Measurement .....	70
3.3.3.3 Energy Model .....	71
3.3.3.4 Results.....	72
4. CONCLUSION.....	77
BIBLIOGRAPHY.....	80

## LIST OF TABLES

Table	Page
1. State-of-the-art sensor node platforms.....	2
2. Parameter settings of the processor and the transceiver .....	33
3. Parameter settings for different scenarios.....	34
4. Balance equations of the queueing model .....	44
5. Network States for a 3-node Sensor Network .....	47
6. Parameter Settings of the Processors and Sensor Nodes .....	72

## LIST OF FIGURES

Figure	Page
1. Illustration of a wireless sensor network used in paper machine .....	3
2. WSN for condition monitoring in aircraft engines .....	4
3. Design layers of WSN .....	5
4. Supply voltage vs. operating frequencies .....	11
5. Power consumption using DVS techniques .....	12
6. Illustration of symbol rate and modulation level in communication .....	14
7. Energy consumption of power amplifier for various modulation level .....	15
8. $E_{comm}$ with respect to communication distance and transmission time .....	15
9. $E_{comm}$ versus transmission time for short communication distance .....	16
10. Dynamic time allocation for single-node scenario .....	17
11. Resultant energy consumption for a single-node scenario .....	18
12. Illustration of a cluster-based WSN .....	22
13. Illustration of the data acquisition scheme in a sensor network .....	23
14. Reservation-based TDMA protocol .....	24
15. Classification of sensor nodes for various communication distances and time constraints .....	30
16. Procedure of Dynamic Time Allocation algorithm .....	31
17. Energy consumption for a 1-node case .....	35
18. Energy consumption for a 2-node case .....	35
19. Energy consumption for various node number and packet sizes .....	36
20. Computation time of the Dynamic Time Allocation algorithm .....	37

21. Three node states of sensor nodes in RWSN .....	40
22. Recharging scheme and area coverage w.r.t. active node density .....	41
23. Queueing network model .....	43
24. Transition process of the queueing model .....	44
25. Time-average area coverage for threshold activation policy .....	45
26. The network state, selected action, and sequential transition process .....	48
27. Recurrence relation of the network states and associated value functions .....	53
28. Network performance for the independent sensor model .....	59
29. Network performance for the correlated sensor model .....	60
30. Network initialization and formation .....	62
31. Cluster head selection process .....	64
32. Time synchronization message over the radio .....	65
33. Hardware architecture of the sensor node .....	68
34. Circuit diagram of the sensor board .....	69
35. Experimental Setup for a reconfigurable sensor network .....	70
36. Measurement circuit for power profiling of sensor nodes .....	71
37. Energy profiling of using reconfiguration and without using reconfiguration technique .....	74
38. Energy consumption with and without node reconfigurability .....	75
39. Energy saving for various sampling frame and node number .....	76





# CHAPTER 1

## INTRODUCTION

### 1.1 Wireless Sensor Networks

A wireless sensor network (WSN) is a network of spatially distributed sensor nodes that communicate wirelessly to cooperatively monitor physical conditions such as temperature, pressure, vibration, or image of a target. In recent years, WSNs have been incorporated into many applications, such as environmental monitoring [1, 2], structural monitoring [3, 4], machine condition monitoring [5], surveillance systems [6, 7, 8], and medical monitoring [9]. The advantages of using WSNs over wired sensing systems include: (1) easy deployment and adaptable network topology (2) no cable installation and maintenance costs and (3) increased portability and network scalability. These distinctive characteristics make WSNs a promising technology. The market potential for WSNs is expected to grow rapidly over the next 5-10 years, particularly in industrial monitoring applications, from its current small base to 5-7 billion dollars [10]. However, the demand for small size and low cost sensor nodes imposes severe challenges in hardware and software design for achieving required network performance. Sensor nodes with hardware constraints in energy source, computational speed, memory capacity, and communication bandwidth have to achieve low energy consumption, short data reporting delay, reliable data communication, and scalable sensor network. Currently, there are several state-of-the-art sensor node platforms available on the market, which separately target different applications as shown in Table 1.

Table 1: State-of-the-Art sensor node platforms

<b>Node Type</b>	<b>Intel Telos</b>	<b>Berkeley Mica2</b>	<b>Sun SPOT</b>	<b>Crossbow Imote2</b>
<b>Example Picture</b>				
<b>MCU Type</b>	8 MHz, 8 bit	8 MHz, 8 bit	180 MHz, 32 bits	13-416 MHz, 16 bits
<b>RAM</b>	2 KB	4 KB	512 KB	256 KB
<b>ROM</b>	256 KB	512 KB	4 MB	32 MB
<b>Bandwidth</b>	250 kbps	38.4 kbps	250 kbps	250 kbps
<b>Battery Capacity</b>	Coin cell 1000 mAh	2xAA 5700 mAh	Rechargeable 750 mAh	3xAAA 3750 mAh

The rapid development in WSNs has created new opportunity for monitoring complex systems, which require large-scale, accurate and timely data acquisition and diagnosis. WSNs are increasingly seen in complex industrial and transportation systems and play an important role in making timely decisions. Industries such as power grid, paper and pulp, oil refinery, and transportation systems need to improve and expand their monitoring systems by using WSNs. In the paper and pulp industry, hundreds of sensors are often needed to monitor the condition of a paper machine and the product quality within the manufacturing process. Effective monitoring systems can prevent unplanned, sudden failure of a machine, thus minimizing economic losses and impact on production.

Figure 1 illustrates the use of a WSN on a paper machine in which multiple sensors are installed to monitor the working status of each of the major sections of the machine.

For example, load sensors embedded within the rollers can monitor tension of the paper web, and humidity sensors can monitor the web moisture content. The ability to use distributed data fusion at the local sensor node (SN) level, instead of passing all raw physical data to the central controller for system-level control sets such a wireless sensor network apart from the conventional approach where individual sensors are connected directly to a central controller. For example, higher humidity measured in the web may require longer drying time, for which the web speed could be decreased to reduce material flow through the drying station, thereby extending the drying period, without the involvement of the central controller. Distributed sensing and sensor coordination will improve system control while reducing communication traffic within the network, and make the operation more energy efficient.

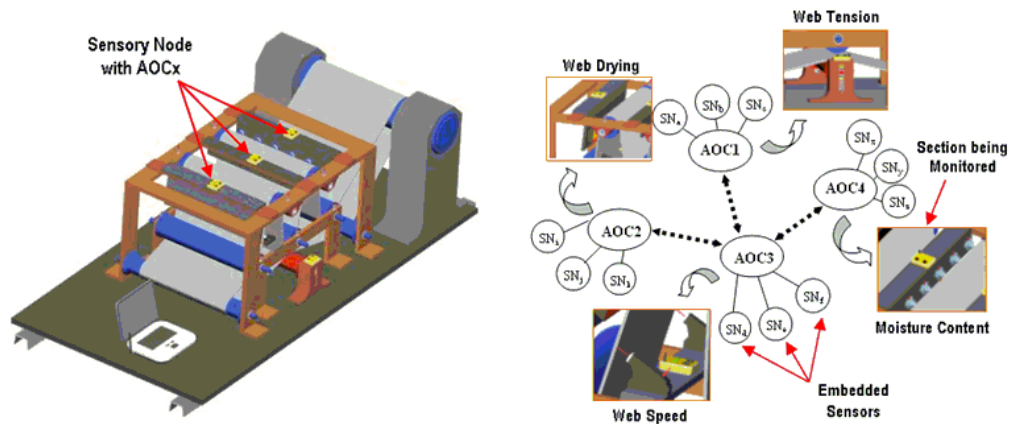


Figure 1: Illustration of a wireless sensor network used in paper machine

In aircraft monitoring systems, a large number of sensors are also needed to monitor performance parameters, such as temperature (inlet, outside air, exhaust gas, turbine), pressure (inlet, compressor, discharge), and vibration (rotors, shafts, reduction gears, bearings) [11] to detect incipient defects and impending failure, reducing

unscheduled delays and serious engine and structure failures. Figure 2 shows the deployment of various sensors on a commercial aircraft engine.

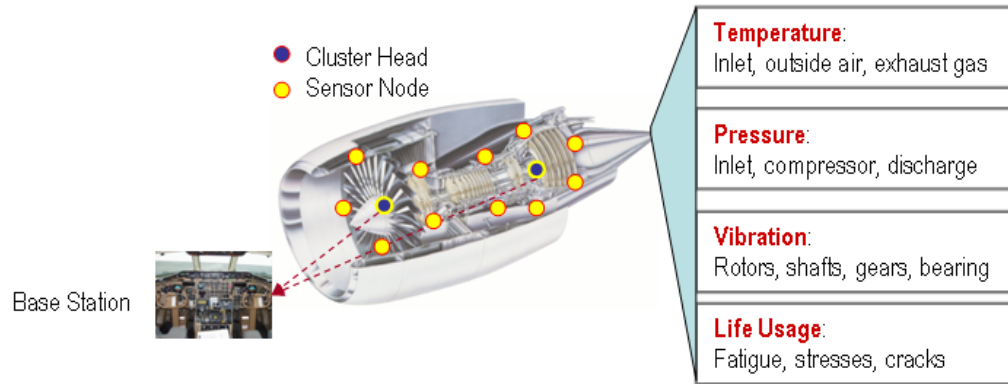


Figure 2: WSN for condition monitoring in aircraft engines

## 1.2 Energy-Efficient Techniques

Reliability and robustness have been the main concerns that prevent the wide adoption of WSNs in realistic applications. To ensure proper functioning of a WSN, the system must be able to provide minimized delays in data communication, high accuracy in data measurement, scalability in expanding the network size, and minimum energy consumption. Of these requirements, minimizing network energy consumption while retaining other network performance metrics imposes a severe challenge in achieving long system life and reducing the frequency of the network maintenance. Researchers have tried to improve energy efficiency of the system by addressing the various constituent layers of WSNs, including hardware platforms and every communication layer as shown in Figure 3. The state-of-the-art techniques for improving energy efficiency include low-power hardware designs [12] and energy-efficient protocols [13], such as routing protocols in the network layer [14], scheduling and contention protocols in the MAC (Media Access Control) layer [15], and multihop communication



protocols in the link layer. However, the use of the above techniques for designing low-power systems based on fixed hardware platforms may not be sufficient for complex system monitoring due to both the requirement for high performance sensor nodes and the requirement for low energy consumption.

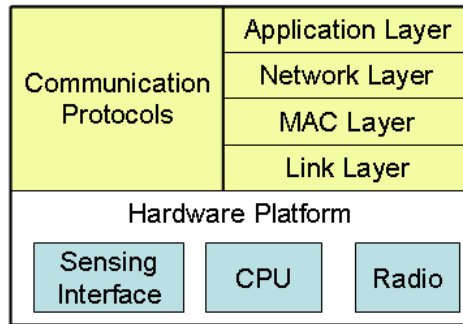


Figure 3: Design layers of WSN

### 1.3 Dynamic Reconfiguration

Recently, techniques of dynamic reconfiguration have attracted increasing attention from the research community. These techniques enable reconfiguration of the sensor network hardware at run time to adapt to external dynamics, providing an innovative approach to designing an energy-efficient WSN in a highly dynamic environment. Due to advances in hardware technology, several reconfiguration techniques have been developed on the sensor node level. These include Dynamic modulation scaling (DMS) (used to reconfigure modulation schemes in communication), dynamic voltage scaling (DVS) (used to reconfigure voltages and operating frequency of processors), adaptive sampling rate (used to change the sampling rate of sensors), and intelligent node activation (used to change sensor node status). The energy efficiency achieved by these dynamic reconfiguration techniques can be categorized into two different types. At node-level reconfiguration, the DVS, DMS, and adaptive sampling rate are used to

minimize the energy consumption of sensor nodes. At network-level reconfiguration, intelligent node activation determines node activity to minimize redundant energy usage within the network. The utilization of all reconfiguration techniques have to consider dynamic factors, such as changes in user requirements, variations in communication channel quality, application changes, addition of new nodes, and node failure. This increases the complexity of using dynamic reconfiguration in WSNs.

#### **1.4 Motivation**

The concept of using dynamic reconfiguration in WSNs is novel. Although the dynamic reconfiguration techniques enable a highly flexible system, the implementation of these techniques in WSN design demands highly complex algorithms. Energy consumption can be reduced more by a simultaneous consideration of DVS and DMS for node-level reconfiguration than the individual use of DVS or DMS. For network-level reconfiguration, a scheduling of node activation to reduce redundant energy usage is critical but has not been well addressed in the literature. Furthermore, an implementation of reconfigurable sensor networks to test their energy efficiency and feasibility has not been conducted in realistic application. These motivate us to investigate the simultaneous utilization of DVS, DMS, and intelligent node activation to achieve a highly energy-efficient sensing system for realistic dynamic environments.

## CHAPTER 2

### PROBLEM STATEMENT

The objective of this research is to develop algorithms for node-level and network-level reconfigurations in order to reduce energy consumption of WSNs. The algorithm developed for node-level reconfiguration was intended to minimize energy consumption by dynamically adjusting the optimal parameter settings of processors and transceivers for every sensor node. The algorithm developed for network-level reconfiguration was aimed at reducing the redundant energy usage of sensor nodes by determining optimal activation decisions, to minimize the maintenance frequency of the network and save cost.

To achieve this objective, mathematical models for the operation of reconfigurable sensor networks at the node level and network level were built first. Then, optimization problems corresponding to each model were formulated whose solutions suggested the optimal configuration of the network. At the node level, an optimization problem for integration of DVS and DMS was formulated; at the network level, a control optimization problem for a stochastic decision process was formulated. The approach to the solutions of these problems were also investigated. The solutions needed to be computationally efficient since they had to run in the sensor nodes in real-time by. In the last stage of the research, an implementation of a reconfigurable sensor network was built to experimentally evaluate the effectiveness of the proposed methodology for dynamic reconfiguration of WSNs.

## **CHAPTER 3**

### **RESEARCH TASKS**

To investigate the dynamic reconfiguration techniques for WSNs, three main research tasks are addressed in this study: the algorithm for node-level reconfiguration, the algorithm for network-level reconfiguration, and an implementation of a reconfigurable sensor network. The following sections in this chapter will separately introduce these tasks and their solution.

#### **3.1 Node-Level Reconfiguration**

The dynamic reconfiguration at node level sought to minimize energy consumption by dynamically adjusting hardware platforms of sensor nodes. We addressed two promising reconfiguration hardware techniques, DVS and DMS, since they have already been separately used on computation and communication systems to reduce the energy consumption. A dynamic time allocation was developed, which considered DVS and DMS simultaneously to fully utilize the energy-aware capability of sensor nodes. In the following sub-sections, the two energy-aware techniques are first introduced, and then the dynamic time allocation is analyzed on a single-node scenario and is extended to multi-node scenario. Simulation results showing the effectiveness of using dynamic time allocation on a machine monitoring application will be demonstrated at the end of the section.

##### **3.1.1 Literature Review**

The concept of lowering voltage and frequency to reduce energy consumption of a computation system was first proposed by Gutnik and Chandrakasan in 1997 [16]. The

utilization of DVS technique required consideration of time constraints because the changes in operating frequency interfered with the computation time given a fixed computation workload. Hence, a scheduling algorithm was usually accompanied with DVS technique to guarantee the time constraint, especially in real-time applications. Researches have worked on scheduling algorithms for using DVS in different applications. In [17, 18], real-time scheduling of computation tasks for a sensor node were proposed to reduce energy consumption in computing stochastic computational tasks. In [19], DVS was used to achieve an energy-efficient WSN for dynamic system monitoring of large-scale and capital intensive machines. Currently, DVS has already been used on digital signal processor (Blackfin, PXA) and sensor node platform (Imote2) to achieve energy efficiency of the system.

DMS was another emerging reconfiguration hardware technique that has been utilized to reduce energy consumption in wireless communication [20, 21], where the communication energy was reduced by changing the modulation level of the communication at the cost of increased transmission time. The concept of changing modulation level on the fly to save the communication energy was first proposed by Schurgers et al. in 2001 [22]. Significant research and development efforts have been made on the scheduling algorithm for DMS to provide significant energy savings while maintaining the time constraints. In [20-27], energy-efficient communication systems were achieved by scheduling random arrival transmission packet of a sensor node. [26] provided algorithmic solutions to the problem of scheduling packet transmission for data gathering in WSN by exploring modulation scaling. In [27], a control scheme was proposed using modulation scaling to minimize energy consumption while ensuring

application qualities. The adaptive modulation has also been used on the new generation broadband wireless protocol, WiMAX (IEEE 802.16 Standard), to optimize the throughput based on the channel conditions. Using DMS technique, higher modulation level was used in communication to increase the throughput when SNR (signal-to-noise ratio) for the receiver was good. The WiMAX system stepped down to lower modulation level when SNR was poor in order to maintain the connection quality and link liability. An implementation of DMS on single chip that suitable for embedded system has also been developed in [28, 29].

While all the above efforts consider single reconfiguration hardware technique, the integration of multiple reconfiguration hardware techniques has not been well addressed in the research community. In [30], the problem of integrating reconfigurable computation and communication was addressed. In this thesis, a detailed DVS and DMS techniques were introduced, and a dynamic time allocation technique used to minimize the total energy consumption within the network was mathematically formulated to tackle the problem.

### 3.1.2 DVS Technique

In CMOS circuits, the average power consumed by a data processor  $P_{comp}$  was proportional to the square of supply voltage  $V$  and operating frequency of the processor  $f$  as [16]:

$$P_{comp} = C \cdot V^2 \cdot f \quad (1)$$

where  $C$  is the effective switching capacitance determined by hardware. Because the speed at which a digital circuit could switch states was proportional to the supply

voltage, the maximum frequency at which the circuit could achieve was determined by the supply voltage. The resultant relation between  $V$  and  $f$  was in the form of:

$$V = \frac{f}{K} + \varepsilon \quad (2)$$

where  $K$  and  $\varepsilon$  are hardware dependent parameters. Therefore,  $P_{comp}$  as a function of  $f$  was proportional to its cube ( $P_{comp} = g(f^3)$ ). Figure 4 illustrates the voltage and frequency relation for Intel Xscale processor (PXA271) [31], where the frequency is scaled from 13MHz to 416 MHz with a minimum supply voltage 0.85V.

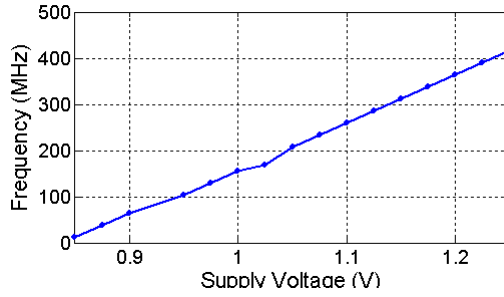


Figure 4: Supply voltage vs. operating frequencies

When computing a fixed task with  $N$  machine cycles required for the task, computation time of the task  $\tau_c$  was:

$$\tau_c = \frac{N}{f} \quad (3)$$

The energy consumption in task computation  $E_{comp}$  was calculated by:

$$E_{comp} = P_{comp} \cdot \tau_c = N \cdot C \cdot \left( \frac{N}{K \cdot \tau_c} + \varepsilon \right)^2 \quad (4)$$

where  $E_{comp}$  decreases quadratically with  $f$ . The energy could thus be reduced by reducing the  $V$  and  $f$  of the processor with longer computation time as the tradeoff.

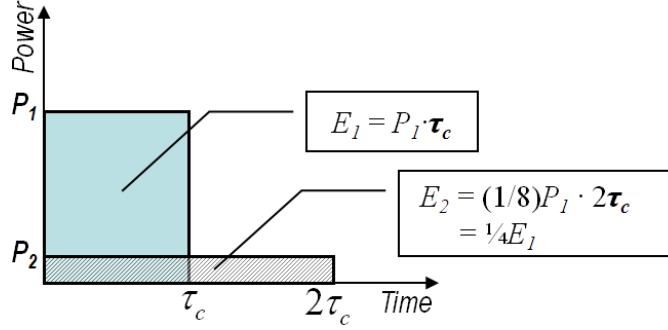


Figure 5: Power consumption using DVS technique

Figure 5 illustrates the power consumption in processing a task for two different time constraints. Assuming a fixed  $N$ -cycle computation task was processed, if the task needed to be finished within computation time  $\tau_c$ , the required operating frequency  $f_1$  was equal to  $N/\tau_c$ , which corresponded to the supply voltage  $V_1$ . The energy consumption used in processing the task  $E_1$  was equal to  $P_1 \cdot \tau_c = N \cdot C \cdot V_1^2$ . However, if the allowable processing time was relaxed to  $2 \cdot \tau_c$ , only half the original operating frequency  $f_2 = 0.5 \cdot f_1$  was required to finish the task. The supply voltage for the new constraint  $V_2$  can be lowered to  $0.5(V_1 + \epsilon) \approx 0.5V_1$ . The new power consumption  $P_2$  and the resultant energy consumption  $E_2$  was:

$$P_2 = C \cdot (V_1/2)^2 \cdot (f_1/2) = P_1/8 \quad (5)$$

$$E_2 = P_2 \cdot 2\tau_c = E_1/4 \quad (6)$$

Hence, the energy consumption in computing the same task was reduced to one fourth of its original value.

### 3.1.3 DMS Technique

DMS exhibited similar energy consumption and processing time tradeoff as DVS, but its energy model was more complex due to the involvement of physical signal



propagation over the air. For transmitting a  $H$ -bit data packet, the total transmission time was determined by the used symbol rate  $R_S$  and modulation level  $b$ . The symbol rate  $R_S$  specified the number of symbols transmitted per unit time. The modulation level  $b$  was the data size that defines a symbol. The multiplication of  $R_S$  and  $b$  was the actual data rate in data communication, and the transmission time  $\tau_t$  was calculated as:

$$\tau_t = \frac{H}{R_S \cdot b} \quad (7)$$

Figure 6 illustrates the significance of  $R_S$  and  $b$  in communication. Under the assumption of fixed symbol rate  $R_S = 1$  symbol/ $10\mu\text{s}$ , a 6-bit packet was transmitted under different modulation levels  $b = 1, 2,$  and  $3$ . Using modulation level  $b = 1$  (i.e. 1 bit/symbol), every bit of data was encrypted into a symbol and six symbols were transmitted in  $60\mu\text{s}$ . The use of  $b = 3$  required only two symbols and  $20\mu\text{s}$  to complete the transmission. Hence, a shorter transmission time was achieved under higher modulation level. To achieve high modulation level, more waveforms were needed to represent a symbol. Quantitatively,  $2^m$  waveforms were required to represent an  $m$ -bit symbol ( $b = m$ ), which were assigned through amplitude, phase and frequency modulations. Illustrated in Figure 6 is a phase modulation of waveforms where each phase corresponds to one signal. The modulation levels that were implemented on the transceiver limited the minimum and maximum transmission time in completing an  $H$ -bit data transmission. According to Equation 7, when  $b \in [b_{min}, b_{max}]$ , the minimum transmission time,  $\tau_{t,min}$ , was equal to  $H/(R_S \cdot b_{max})$  and the maximum transmission time,  $\tau_{t,max}$ , was equal to  $H/(R_S \cdot b_{min})$ .

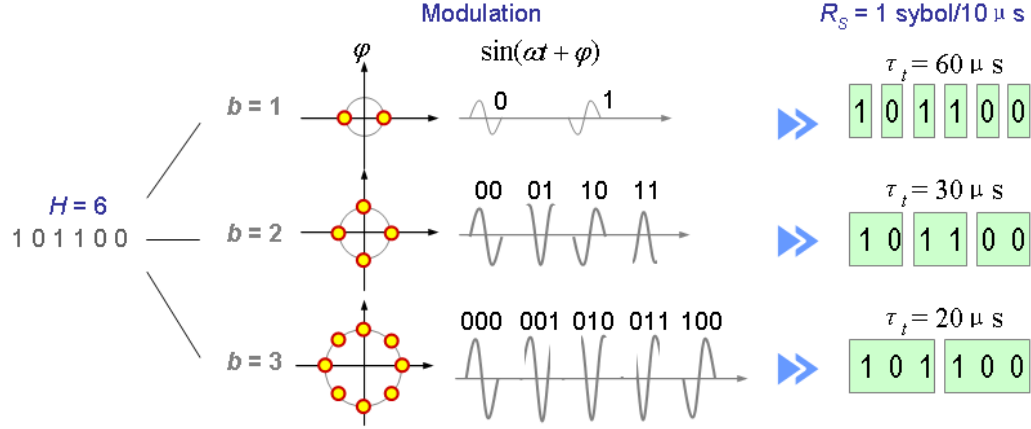


Figure 6: Illustration of symbol rate and modulation level in communication

High modulation level for data communication lead to a high transmitting power in order to meet the required signal-to-noise ratio at the receiver. Under the assumption of a free space channel and uncoded M-ary Quadrature Amplitude Modulation (MQAM) [32, 33], the communication energy,  $E_{comm}$ , consumed for data transmission was calculated as [20]:

$$E_{comm} = F \cdot r^2 \cdot (2^{H/(R_s \cdot \tau_t)} - 1) \cdot R_s \cdot \tau_t + G \cdot R_s \cdot \tau_t \quad (8)$$

where  $F$  and  $G$  are hardware constants and  $r$  is the communication distance. The term  $F \cdot r^2 \cdot (2^{H/(R_s \cdot \tau_t)} - 1) \cdot R_s \cdot \tau_t$  in Equation 8 represents the energy consumption of the power amplifier, which increases with modulation level  $b$  as illustrated in Figure 7.

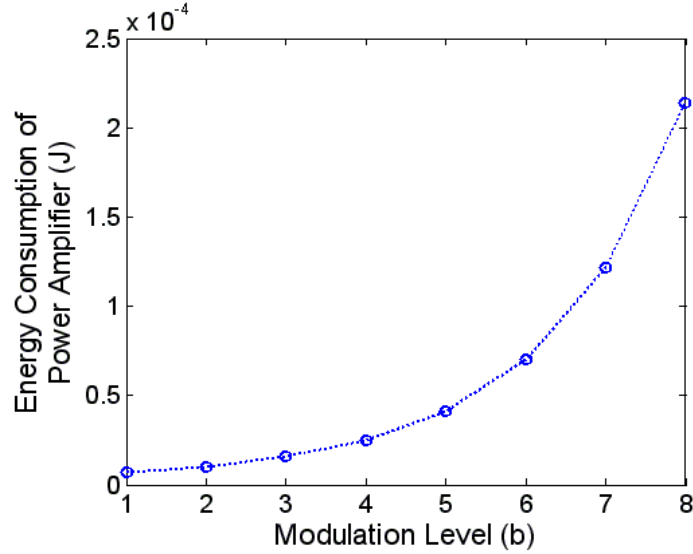


Figure 7: Energy consumption of power amplifier for various modulation level

The term  $G \cdot R_S \cdot \tau_t$  in Equation 8 accounts for the energy used in the remaining transceiver circuits. Since the power consumptions of the circuits were independent of the communication distance, the energy consumption of these circuits was linearly proportional to the transmission time. That means that energy is consumed if shorter transmission times are used in communication. Figure 8 illustrates the total energy consumption for various  $r$  and  $\tau_t$ .

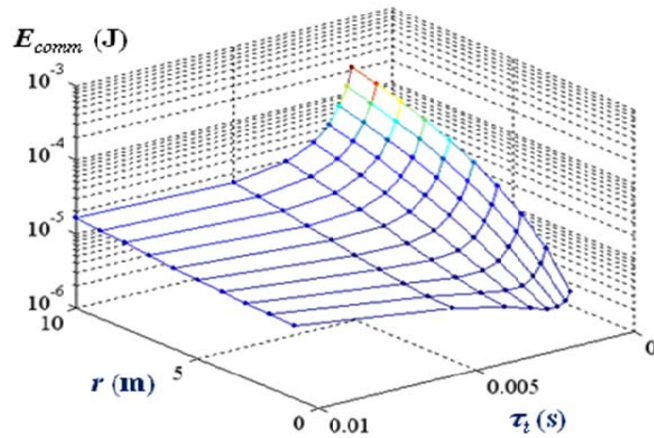


Figure 8:  $E_{comm}$  with respect to communication distance  $r$  and transmission time  $\tau_t$  ( $R_S = 100$  kBaud,  $H = 1000$  bits,  $b = \{1, \dots, 8\}$ )

In long-range data communication, the power amplifier dominated the total energy consumption, so the communication energy monotonically decreased as the transmission time  $\tau_t$  increases. However, in short-range data communication, such as  $r = 1$  in Figure 9, the energy function became concave with respect to  $\tau_t$  because the energy consumption of the power amplifier was comparable to the other transceiver circuits. Therefore, an optimal transmission time existed, which resulted in the least energy consumption due to the two different transceiver components.

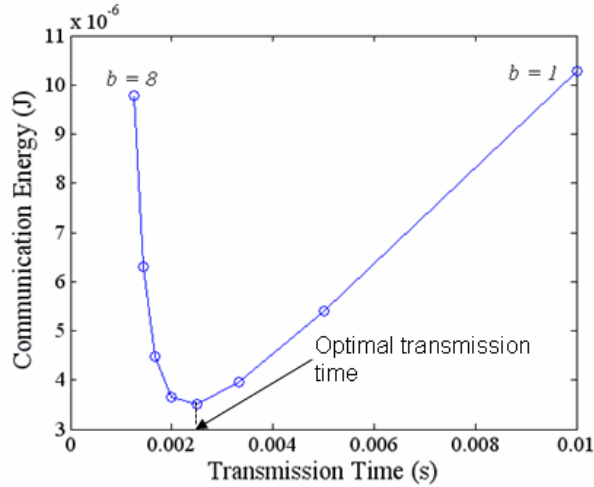


Figure 9:  $E_{comm}$  versus transmission time for short communication distance ( $r = 2$  m)

### 3.1.4 Dynamic Time Allocation

Since both DVS and DMS techniques traded energy savings against the computation and communication time, respectively. When only limited time was available for the sensor node, it became critical to allocate the time resource for minimizing the total energy consumption. Such an allocation mechanism was called Dynamic Time Allocation (DTA), which determined the optimal share of computation time and transmission time subject to the time constraint. In this section, the DTA is

first analyzed from a single-node scenario, and then extended to multi-node scenario. A DTA algorithm that efficiently solved the formulated optimization problem was developed at the end to determine the optimal parameter settings for every sensor node.

### 3.1.4.1 Single-Node Scenario

Figure 10 illustrates a single-node scenario where a sensor node locally computes the task and transmits the data to base station. Under the time constraint  $d$ , the sum of computation time  $\tau_c$  and communication time  $\tau_t$  was equal to  $d$  for fully utilizing the available time.

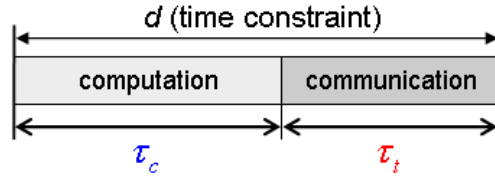


Figure 10: Dynamic time allocation for single-node scenario

When DVS and DMS techniques were both used on the sensor node, the respective energy consumption,  $E_{comp}$  (computation energy) and  $E_{comm}$  (communication energy) varies with  $\tau_c$  and time  $\tau_t$ . Figure 11(a) illustrates the  $E_{comp}$  as a function of  $\tau_c$ , where  $E_{comp}$  decreased with increasing  $\tau_c$ . Because the available operating frequency of the processor was bounded by  $f_{min}$  and  $f_{max}$  due to the processor capability, when the allowable processing time was shorter than  $N/f_{max}$ , the processor was not be able to finish the computation task within the required time. On the other hand, when the allowable processing time was longer than  $N/f_{min}$ , the processor operates at  $f_{min}$  to consumed the least energy. Figure 11(c) illustrates  $E_{comm}$  as a function of  $\tau_t$ , where  $E_{comm}$  decreased with increasing  $\tau_t$  and decreasing communication distance  $r$ . Due to the

available modulation level of the radio, the  $\tau_t$  that could be achieved by the radio was restricted between  $H/(b_{max} \cdot R_S)$  and  $H/(b_{min} \cdot R_S)$ . Specifically, the achievable  $\tau_c$  and  $\tau_t$  were discrete as the dots indicated in Figures 11(a) and 11(c). The discrete value of  $\tau_c$  was caused by the resolution of the voltage regulator, where each supply voltage corresponded to specific operating frequency. The discrete value of  $\tau_t$  resulted from the discrete modulation level of the radio.

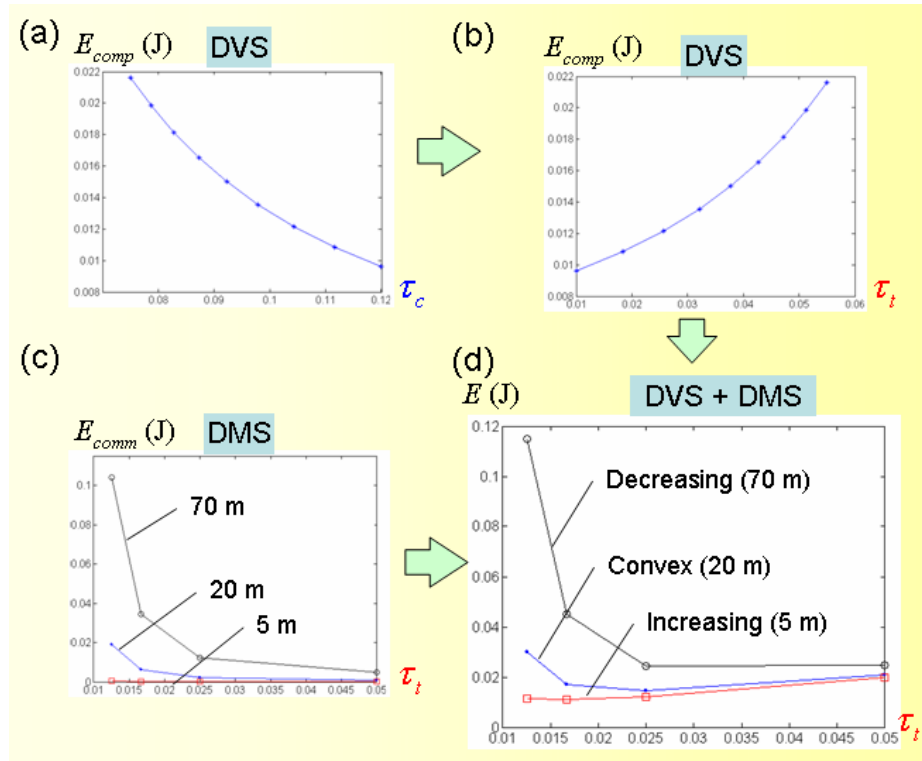


Figure 11: Resultant energy consumption for a single-node scenario

Under the time constraint  $d$ ,  $\tau_c$  and  $\tau_t$  were coupled to each other. When  $d$  was larger than  $H/(b_{min} \cdot R_S)$  plus  $N/f_{min}$ , the available time resource allowed both the processor and the radio operating at the maximum  $\tau_c$  and  $\tau_t$ , so a minimum energy was achieved. However, when  $d$  was smaller than  $H/(b_{min} \cdot R_S)$  plus  $N/f_{min}$ , it became necessary to determine the optimal share of time resource. The  $E_{comp}$  as a function of  $\tau_c$

( $= d - \tau_t$ ) was converted to  $\tau_t$  as shown in Figure 11(b), so the representation of time allocation could be indicated by a single variable  $\tau_t$ . The reason to choose  $\tau_t$  rather than  $\tau_c$  was because  $\tau_t$  had fewer discrete values which reduced the dimension of the optimization problem. Depending on the communication distance  $r$ , the resultant energy consumption  $E$  ( $= E_{comp} + E_{comm}$ ) as a function of  $\tau_t$  exhibited three characteristics: monotonically increasing, monotonically decreasing, and convex functions as illustrated in Figure 11(d). The monotonically increasing function occurred in short communication distance, where the  $E_{comp}$  dominated the total energy consumption, so the behavior of  $E$  was similar to  $E_{comp}$ . The monotonically decreasing function occurred in long communication distance, where the  $E_{comm}$  dominated the total energy consumption, so the behavior of  $E_t$  was close to  $E_{comm}$ . As for the intermediate communication distance, a convex function was formed due to the two comparable energy functions,  $E_{comp}$  and  $E_{comm}$ . An optimization problem that minimizing the total energy consumption in a single-node scenario was formulated as:

$$\begin{aligned} \min E(\tau_t) &= N \cdot C \cdot \left( \frac{N}{K \cdot (d - \tau_t)} + \varepsilon \right)^2 \\ &\quad + [F \cdot r^2 \cdot (2^{H/(R_s \cdot \tau_t)} - 1) + G] \cdot R_s \cdot \tau_t \\ \text{Subject to} & \\ \tau_t &= \frac{H}{R_s \cdot b} \\ b &= \{2, 4, 6, 8\} \end{aligned} \tag{9}$$

where the solution (optimal transmission time) can be derived by solving:

$$dE(\tau_t)/d\tau_t = 0 \tag{10}$$

$$\frac{d^2E}{d\tau_t^2}(\tau_t) > 0 \tag{11}$$

where Equation 11 proves the convexity of the energy function. Since only the sensor node whose energy function was convex was required to solve the above optimization problem. As for the sensor node whose energy function was monotonically decreasing or decreasing,  $\tau_{t,min}$  ( $= H/(b_{max} \cdot R_S)$ ) and  $\tau_{t,max}$  ( $= H/(b_{min} \cdot R_S)$ ) could be directly determined as the optimal transmission. By finding the critical communication distances that distinguished the three energy function, the computational complexity in finding the optimal transmission time was reduced. The critical communication distance was derived by considering Equation 10 in the form of:

$$E'_{comp} + G \cdot R_S - F \cdot R_S \cdot r^2 \cdot [1 - 2^{H/(R_S \cdot \tau_t)} \cdot (1 - 0.693H/(R_S \cdot \tau_t))] = 0 \quad (12)$$

$$E'_{comp} = \frac{dE_{comp}}{d\tau_t} = \frac{2N^2 \cdot C}{K \cdot (d - \tau_t)^2} \left( \frac{N}{K \cdot (d - \tau_t)} + \varepsilon \right) \quad (13)$$

The  $r$  that satisfied Equation 12 was required to be:

$$r = \sqrt{\frac{E'_{comp} + G \cdot R_S}{F \cdot R_S \cdot [1 - 2^{H/(R_S \cdot \tau_t)} \cdot (1 - 0.693H/(R_S \cdot \tau_t))]} = g(\tau_t) \quad (14)$$

where function  $g$  as a function of  $\tau_t$  is a non-decreasing function. Because  $\tau_t$  was bounded by  $\tau_{t,min}$  and  $\tau_{t,max}$ , the  $r$  that satisfied Equation 14 was also bounded by  $g(\tau_{t,min})$  and  $g(\tau_{t,max})$ . Therefore, only the sensor node whose  $r$  within  $g(\tau_{t,min})$  and  $g(\tau_{t,max})$  exhibited a convex energy function. For the sensor node whose  $r$  was smaller than  $g(\tau_{t,min})$ ,  $dE/d\tau_t$  was positive over all  $\tau_t$ , which corresponded to the monotonically increasing energy function. When  $r$  was larger than  $g(\tau_{t,max})$ ,  $dE/d\tau_t$  was negative over all  $\tau_t$ , which corresponded to a monotonically decreasing energy function. This classification technique was used to reduce the optimization complexity in the multi-node scenario.



#### **3.1.4.2 Multi-Node Scenario**

The utilization of DTA in multi-node scenario was more complex since the utilization of the available time resource depended on the chosen data acquisition scheme and communication protocol. A real-time data acquisition was considered where sensor nodes in the sensing field continuously monitored the environmental phenomena and the collected data needed to be reported to the base station under the time constraint. Unlike event-driven application where random access could be used in the MAC (Medium Access Control) layer; such type of scenario requires channel partitioning of the MAC layer to offer a stable network structure in sustaining consistent data load. In this section, a data acquisition scheme and the MAC protocol suitable for the efficient utilization of DTA is investigated, and then an optimization problem is formulated to minimize the energy consumption of the network.

#### **3.1.4.3 Network Sectioning**

It has been investigated [5, 34] that sectioning of the WSN allowed for improved computational efficiency in aggregating information to reduce the communication energy. Figure 12 illustrates such cluster-based WSN, where sensor nodes are grouped into multiple *clusters* with a randomly chosen *cluster head* in each cluster. Every cluster head collected the extracted data from every sensor node in the same cluster and aggregated the information (which was called data fusion) to reduce the communication energy.

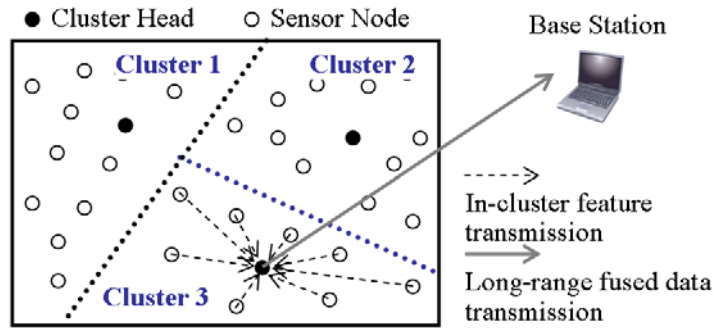


Figure 12: Illustration of a cluster-based WSN

#### 3.1.4.4 Data Acquisition Scheme

Based on the cluster-based WSN, every sensor node kept sampling physical signals and periodically extracted and transmitted the useful information to the cluster head. The cluster head then fused all collected information and transmitted the fused data to the remote base station. To achieve a real-time data acquisition, the time was divided into a series of consecutive *sampling period*  $T$  where all the above tasks had to be performed within each sampling period for the following tasks to be executed in time. In addition, a parallel processing was utilized on every sensor node where raw data were alternatively stored in a dual memory buffer, and the data collected in the previous sampling period were processed within the current sampling period. Figure 13 illustrates a complete data acquisition scheme, which includes all the necessary tasks in individual sampling period.

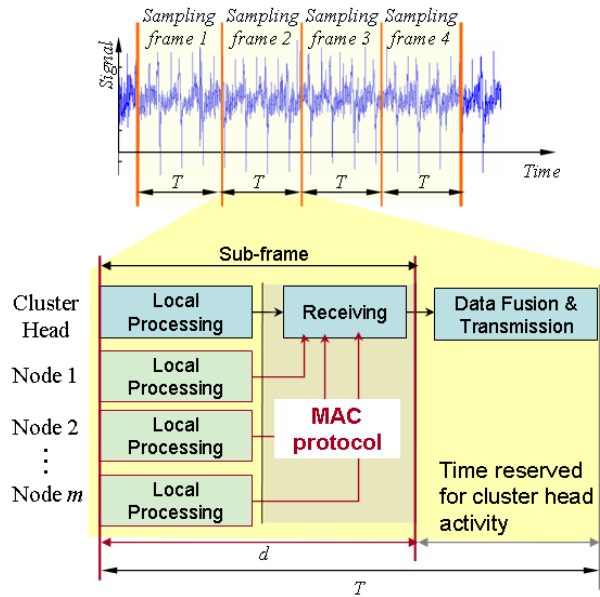


Figure 13: Illustration of the data acquisition scheme in a sensor network

### 3.1.4.5 Communication Protocol

To enable an in-cluster data communication, a reservation-based Time Division Multiple Access (TDMA) protocol [35] was utilized to schedule the multiple access communication. The advantage of using TDMA over FDMA (Frequency Division Multiple Access) lied on its scalability, which allowed more sensor nodes to be accommodated in a cluster, since only limited channel bandwidth was available for the network. The radio circuits that implemented TDMA were simpler compared with CDMA (Code Division Multiple Access), which resulted in lower cost of sensor nodes. Another advantage of using TDMA was its improved energy efficiency through the cooperation of DTA, which was described as follows.

The improved energy efficiency of using TDMA came from its data communication structure. In the reservation-based TDMA protocol, the time was divided into time frames as long as the sampling frame  $T$ . Each sampling frame was

composed of two parts: a *control sub-frame* and a *data sub-frame* as illustrated in Figure 14. The control sub-frame was used for the exchange of control signals including time synchronization, channel quality estimation, and the broadcasting of channel allocation from the cluster head between the cluster head and the other sensor nodes. Furthermore, new added sensor nodes could use the control sub-frame to join the cluster, which increased the network scalability. The data sub-frame reserved for data transmission was divided into time slots with variable length. The cluster head assigned the time slots of all sensor nodes in its cluster in which every sensor node was assigned the whole band of frequencies in a given time slot.

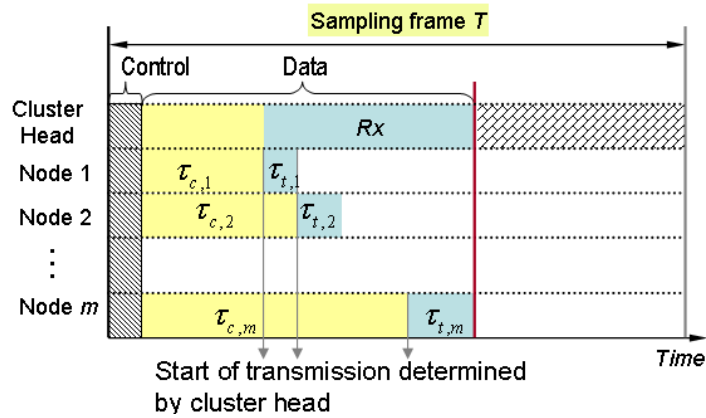


Figure 14: Reservation-based TDMA protocol

In the protocol, every sensor node only turned on its radio during the control sub-frame and the assigned time slot. Such communication structure resulted in energy savings from two aspects: first, the sensor nodes did not need to turn on the radio all the times; second, the unused time slots before data transmission could be completely distributed to the computation task, so DVS could exploit the time to reduce the energy consumption. Every sensor node's transmission time not only determined its local time allocation among  $\tau_c$  and  $\tau_t$ , but also influenced other sensor nodes' total processing time.

For example, when the transmission time of sensor node  $m$ ,  $\tau_{t,m}$ , increased 1 ms, either the computation time of sensor node  $m$ ,  $\tau_{c,m}$ , or the total processing time for sensor nodes  $1 \sim m-1$  had to be decreased 1 ms as well. The utilization of DTA thus had to be considered from the whole cluster to achieve minimum energy consumption of the network.

### 3.1.4.6 Solution Formulation

To achieve a DTA in multi-node scenario, an optimization problem was formulated according to the presented data acquisition scheme and MAC protocol. The objective function of the problem was the total energy consumption of the cluster,  $E_{total}$ , and was expressed as:

$$\begin{aligned}
 E_{total} &= \sum_{i=1}^m [E_{comp}(\tau_{c,i}) + E_{comm}(\tau_{t,i})] \\
 &= \sum_{i=1}^m \left\{ N \cdot C \cdot \left( \frac{N}{K \cdot \tau_{c,i}} + \varepsilon \right)^2 + [F \cdot r_i^2 \cdot (2^{H/(R_S \cdot \tau_t)} - 1) + G] \cdot R_S \cdot \tau_t \right\}
 \end{aligned} \tag{15}$$

where the allowable computation time for sensor node  $i$ ,  $\tau_{c,i}$ , was calculated by:

$$\tau_{c,i} = d - \sum_{j=i}^m \tau_{t,j} \tag{16}$$

The symbol  $d$  referred to the time constraint, where all local computation and in-cluster data communication had to be finished by  $d$  for the following cluster head operation. The control variables of the objective function were converted from transmission time  $\tau_t$  to modulation level  $b$ , because the modulation level was the actual control parameter of the radio. An optimization problem could be formulated as:

$$\begin{aligned}
\min E_{total} &= \sum_{i=1}^m \{E_{comp}(\tau_{c,i}) + E_{comm}(\tau_{t,i})\} \\
&\sum_{i=1}^m \{N \cdot C \cdot (\frac{N}{K \cdot \tau_{c,i}} + \epsilon)^2 + [F \cdot r_i^2 \cdot (2^{H/(R_s \cdot \tau_{t,i})} - 1) + G] \cdot R_s \cdot \tau_{t,i}\} \\
\text{Subject to} & \tag{17} \\
C1: \tau_{c,i} &\geq N / f_{max} \quad (\text{Set by CPU}) \\
C2: b_i &\in \{2, 4, 6, 8\} \quad (\text{Set by radio}) \\
C3: \tau_{c,i} &= d - \sum_{j=i}^m \tau_{t,i} \quad (\text{Set by time scheduling}) \\
C4: \tau_{t,i} &= H / (R_s \cdot b_i)
\end{aligned}$$

The constraint  $C1$  was imposed by the processor capability, which indicated a sensor node's minimum computation time given the maximum operating frequency  $f_{max}$ . The constraint  $C2$  came from the radio limitation that only finite modulation levels were applicable in the communication. The solution to the optimization problem was therefore a set of modulation levels for all sensor nodes, which produced the optimal time allocation. To solve such an integer programming problem, the exhaustive enumeration method was only applicable for small-scale network since the computational loads increased exponentially with respect to the sensor node numbers; the non-linear objective function and the discrete variables precluded the use of calculus-based optimization techniques. Thus, it became significant to derive the optimal result efficiently for the utilization of DTA.

### 3.1.4.7 Dynamic Time Allocation Algorithm

A Dynamic Time Allocation (DTA) algorithm for solving the optimization problem was developed based on the structure of the objective function and the previous classification technique. The algorithm was implemented by the cluster head when the network was subjected to external dynamics, such as node failure, new added node, or

variation in communication condition, so the time allocation could be dynamically updated to maximize the energy efficiency.

The transmission sequence of sensor nodes in a cluster was first determined. Considering the sensor node  $i$  used high modulation level in transmitting the data, the total energy consumption in computation could be decreased due to the prolonged computation time for the sensor node  $i$  and the prolonged processing times for the sensor node 1 to sensor node  $i-1$ . Therefore, the later the transmission sequence where the sensor node  $i$  was located, the higher energy saving could be achieved because more sensor nodes could be benefited from the prolonged processing time. The use of high modulation level caused an increment of communication energy of the sensor node  $i$ , which was proportional to the communication distance between the sensor node  $i$  and the cluster head. Hence, it was more energy efficient to schedule a sensor node with short communication distance in the later transmission sequence, because only minor energy overhead in communication was incurred. The transmission sequence of sensor nodes was therefore scheduled in a decreasing order in terms of the communication distance  $r$ , i.e.,  $r_1 \geq r_2 \geq \dots \geq r_m$ .

After the determination of transmission sequence, a necessary condition for the solution of the optimization problem (the optimal modulation level for every sensor node) was derived stating that the modulation levels for the sensor nodes,  $b_1, b_2, \dots, b_m$ , must appear in a non-decreasing order. This statement was mathematically expressed as Lemma 1.

Lemma 1: Given  $r_i \geq r_{i+1}$  for  $i = 1, \dots, m-1$ , a necessary condition for optimality of

Equation 17 was  $b_i \leq b_{i+1}$ .

Proof: Let  $\vec{\beta}$  be a possible solution such that  $b_i = x$ ,  $b_{i+1} = y$ , and  $x > y$  for  $i \in \{1, \dots, m-$

$1\}$ . Further, suppose that  $\vec{\beta}$  was the optimal solution of the optimization

problem. Consider another possible solution  $\vec{\alpha}$  such that  $b_i = y$ ,  $b_{i+1} = x$ , and  $\alpha_j$

$= \beta_j$  for  $j \neq i, i+1$ . Compare the value of the objective function computed from  $\vec{\beta}$

and  $\vec{\alpha}$ , we obtained:

$$E_{total}(\vec{\beta}) - E_{total}(\vec{\alpha}) = \left[ E_{comp,i+1}(\vec{\beta}) - E_{comp,i+1}(\vec{\alpha}) \right] + H \cdot F \cdot (r_i^2 - r_{i+1}^2) \left[ \frac{2^x - 1}{x} - \frac{2^y - 1}{y} \right] > 0 \quad (18)$$

The inequality contradicted the optimality of  $\vec{\beta}$ , so the optimal solution must

abide by the condition  $b_i \leq b_{i+1}$ . for  $i = 1, \dots, m-1$ . ■

According to Lemma 1, only the vector that satisfied the criterion  $b_1 \leq b_2 \leq \dots \leq b_m$  were considered to be the possible solution. So the number of possible solutions were drastically reduced to  $C_{n_b-1}^{m+n_b-1}$ , where  $m$  was the total sensor node numbers in a cluster and  $n_b$  was the number of available modulation levels of the radio. In our case, where four different modulation levels were available, the possible solutions were efficiently reduced to  $\frac{1}{6}(m+3) \cdot (m+2) \cdot (m+1)$  compared with the exhaustive enumeration, which generated  $4^m$  possible solutions.

Furthermore, the classification technique developed in the single-node scenario was applied to reduce the computational loads in finding the optimal solution. The concept



was to filter out the sensor nodes whose energy function with respect to the transmission time were monotonically increasing or monotonically decreasing and to assign the optimal modulation level  $b_{max}$  or  $b_{min}$  directly. The dimension of the optimization problem could therefore be further reduced.

Since the communication distance of sensor nodes were arranged in a decreasing order, the classification of sensor nodes with monotonically decreasing energy function (appeared in the long communication distance) was analyzed from the sensor node 1; the classification of sensor nodes with monotonically increasing energy function (appeared in the short communication distance) was analyzed from the sensor node  $m$ . The classification was performed according to Equation 14. Given specific time constraint ( $d$  second), if a sensor node's communication distance  $r$  was larger than  $g(\tau_{t,max})$ , the energy function of the sensor node was monotonically decreasing; if  $r$  was smaller than  $g(\tau_{t,min})$ , the energy function of the sensor node was monotonically increasing. The critical communication distances,  $g(\tau_{t,min})$  and  $g(\tau_{t,max})$  that classified the three energy functions varied with  $d$  as illustrated in Figure 15. The classification of a sensor node was thus determined by a sensor node's  $r$  and  $d$ .

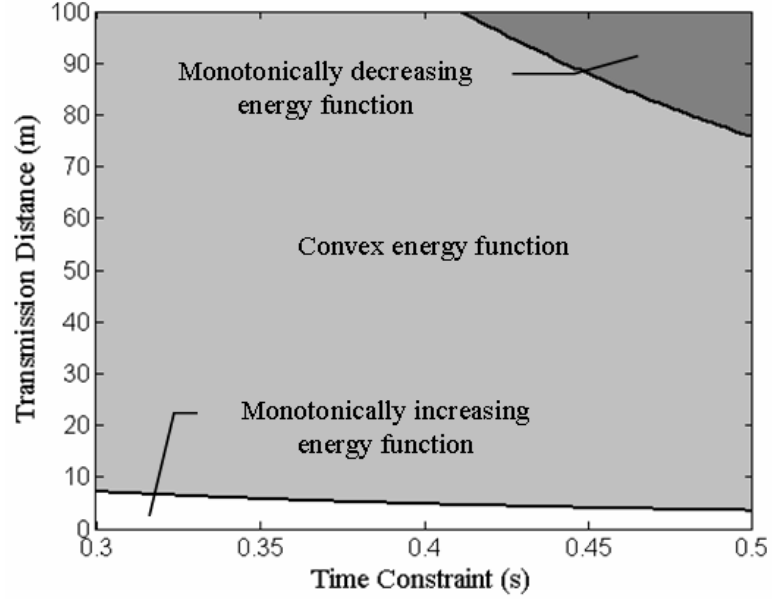


Figure 15: Classification of sensor nodes for various communication distances and time constraints ( $H = 1000$  bits,  $N = 1.1 \times 10^8$ ,  $b_{min} = 2$ ,  $b_{max} = 8$ )

The procedure of classifying the sensor nodes with monotonically increasing energy function was performed backward from the sensor node  $m$ . Given the communication distance  $r_m$  and the time constraint  $d$  for the sensor node  $m$ , the classification of sensor node  $m$  as monotonically increasing energy function was determined by its position on the classification diagram shown in Figure 15, and was mathematically expressed as  $r_m < g(\tau_{t,min})$  given time constraint  $d$ . If the sensor node  $m$  was classified as the sensor node with monotonically increasing energy function, a transmission time,  $\tau_{t,min}$ , was assigned to the sensor node  $m$ . The procedure then continued to classify the sensor node  $m - 1$  with time constraint  $d - \tau_{t,min}$ . The classification continued until a sensor node was classified as the sensor node with convex energy function.

The classification of sensor nodes with monotonically decreasing energy function was performed from the sensor node 1. The time constraint for the sensor node 1,  $d_1$ ,

varied within  $d - (m-1) \cdot \tau_{t,max}$  and  $d - (m-1) \cdot \tau_{t,min}$  depending on the transmission times of the sensor nodes 2 ~ m. If the sensor node 1 was classified as the sensor node with monotonically decreasing energy function given the shortest possible time constraint  $d - (m-1) \cdot \tau_{t,max}$ , the sensor node 1 would have monotonically decreasing energy function over all possible time constraints. The classification of the sensor node 1 as the sensor nodes with monotonically decreasing energy function was then determined by  $r_1 > g(\tau_{t,max})$  given time constraint  $d - (m-1) \cdot \tau_{t,max}$ . If the sensor node 1 was classified as the sensor nodes with monotonically decreasing energy function, the procedure continued to classify the sensor node 2 with time constraint  $d - (m-2) \cdot \tau_{t,max}$ . The classification proceeded until a sensor node was classified as the sensor node with convex energy function.

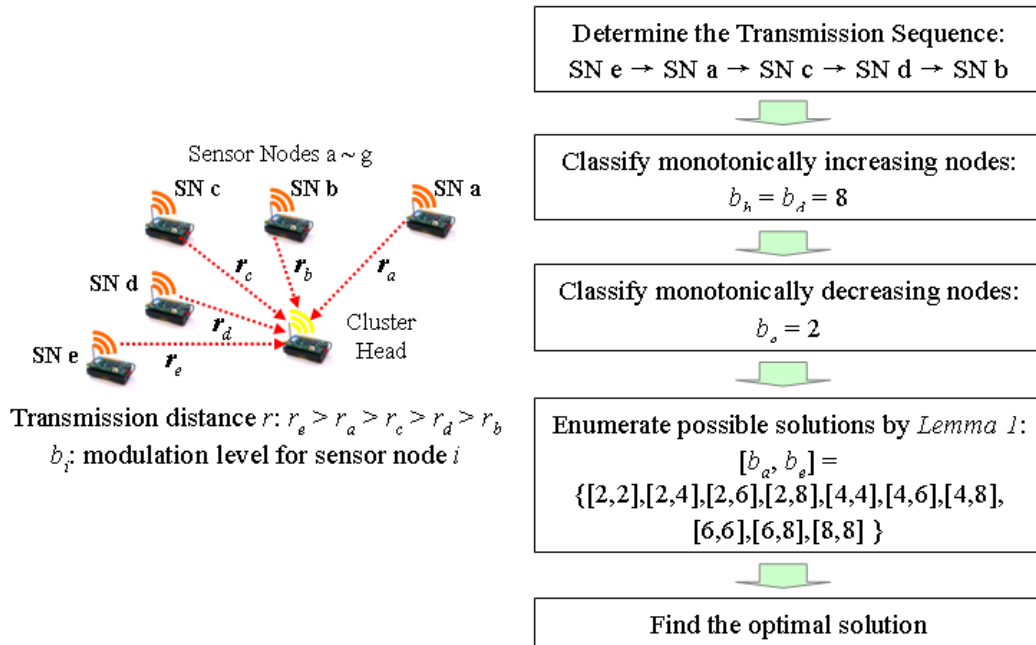


Figure 16: Procedure of Dynamic Time Allocation algorithm

Based on the Lemma 1 and the classification technique, a DTA algorithm was developed to find the optimal solution of the optimization problem efficiently, so the

cluster head could dynamically generate the optimal time allocation for the network. Figure 16 illustrates a complete procedure of performing the DTA algorithm. First, the cluster head acquired the communication distance from the estimation of the link quality for every sensor node, and then scheduled the transmission sequence of sensor nodes in a decreasing order in terms of the communication distance. The classification technique was utilized to filter the sensor nodes with monotonically increasing energy function and the sensor nodes monotonically decreasing energy functions. The optimal modulation level  $b_{max}$  and  $b_{min}$  were assigned directly. For the remaining sensor nodes whose modulation levels had not been determined, the possible solutions were reduced according to the Lemma 1, and found the optimal solution that produced the minimal objective function.

### 3.1.5 Simulation Model and Results

The energy efficiency of using DTA in the multi-node scenario was presented in this section. A real-time machine monitoring application was considered where sensor nodes constantly monitored the vibration signals, which were processed by using the Discrete Harmonic Wavelet Packet Transform (DHWPT) algorithm [51] to extract the desired information. The data processing was performed locally on the sensor nodes to reduce the energy consumption in transmitting the raw data. The extracted data (energy at each sub-frequency band) of every sensor node were collected by the cluster head, and the data were fused on-line by the cluster head to diagnose the machine conditions. The energy consumption of a single cluster was simulated on the MATLAB, where sensor nodes were randomly deployed on a 20 x 20 m<sup>2</sup> sensing area considering the

indoor transmission range of the radio. Assuming the required sampling frame was 1 second, the time reserved for the control sub-frame, data fusion, and data transmission to the base station was 0.5 seconds, so all the tasks for local processing and in-cluster data communication needed to be finished within 0.5 second. The processor and the transceiver used in the simulation were Intel Xscale PXA271 [31] and the parameters of the transceiver were derived from [36]. Table 2 lists the parameters used for the processor and the transceiver, and the related parameters of the application.

Table 2: Parameter settings of the processor and the transceiver

Parameters	Value
<b>Processor Parameters</b>	
<b>Switching Capacitance <math>C</math></b>	1.45 nF
<b>Hardware Parameter <math>K</math></b>	$870 \times 10^6$ MHz/V
<b>Hardware Parameter <math>\varepsilon</math></b>	0.83 V
<b>Maximum Frequency <math>f_{max}</math></b>	412 MHz
<b>Minimum Frequency <math>f_{min}</math></b>	13 MHz
<b>Transceiver Parameters</b>	
<b>Symbol Rate <math>R_S</math></b>	$1.0 \times 10^5$ symbols/second
<b>Hardware Parameter <math>G</math></b>	10 nJ/symbol
<b>Hardware Parameter <math>F</math></b>	67 pJ/symbol/m <sup>2</sup>
<b>Application Parameters</b>	
<b>Computation task <math>N</math></b>	$1.1 \times 10^8$ cycles
<b>Communication task <math>H</math></b>	1000 bits
<b>Sampling Period <math>T</math></b>	1 second
<b>Time Constraint <math>d</math></b>	0.5 second

The effects of the dynamic time allocation on energy reduction were investigated under different cases. In the first case, the number of sensor nodes contained in the cluster varied with unchanged communication and computation tasks. Three different hardware designs were considered: without hardware reconfigurability, with only DVS, and with combined DVS and DMS. In the scheme which without using hardware reconfigurability, the sensor nodes used fixed hardware settings, maximum operating

frequency  $f_{max}$  and minimum modulation level  $b_{min}$ , in processing the tasks. In the scheme where only DVS was utilized, the operating frequency and the supply voltage are adjustable, but only the minimum modulation level  $b_{min}$  was used in the communication. In the scheme where both DVS and DMS were used simultaneously, DTA was applied to obtain the optimal parameter settings for every sensor node. The number of sensor nodes was simulated from 1 to  $m_{max} = 45$ , where  $m_{max}$  is the maximum number of sensor node a cluster could accommodate when no DMS was utilized on the sensor nodes. The value of  $m_{max}$  could be calculated from:

$$\tau_{c,1} \geq d - \sum_{i=1}^m \tau_{t,i} \Rightarrow m \geq \frac{b_{min} \cdot R_S}{H} \left( d - \frac{N}{f_{max}} \right) = m_{max} \quad (19)$$

To evaluate the energy efficiency of the proposed node-level reconfiguration technique, three scenarios were simulated using different level of reconfigurability as shown in Table 3. In the first scenario, sensor nodes without DVS and DMS techniques operated at the maximum supply voltage, maximum operating frequency, and minimum modulation level. In the second scenario, sensor nodes only used DVS technique to reconfigure supply voltage and operating frequency. The minimum modulation level was used in communication. In the third scenario, sensor nodes with DMS and DVS capabilities could reconfigure the supply voltage, operating frequency, and modulation level.

Table 3: parameter settings for different scenarios

Scenario	Voltage	Frequency	Modulation
<b>Scenario 1: No DVS &amp; DMS</b>	1.25V	416 MHz	2
<b>Scenario 2: DVS only</b>	0.85~1.25V	13~416 MHz	2
<b>Scenario 3: DMS + DVS</b>	0.85~1.25V	13~416MHz	2,4,6,8

In a single-node scenario, only one sensor node (Node 1) performed local computation and transmits the data to the cluster head, as shown in Figure 17. The minimum energy consumption was achieved by using  $b = 4$  in the third scheme.

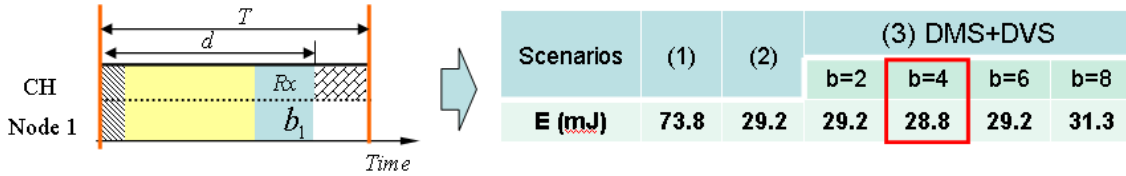


Figure 17: Energy consumption for a 1-node case

In a 2-node case as shown in Figure 18, there were 16 possible time allocations of the network, where the minimum energy consumption was achieved by selecting modulation level of Node 1,  $b_1$ , equal to 4 and selecting modulation level of Node 2,  $b_2$ , equal to 6.

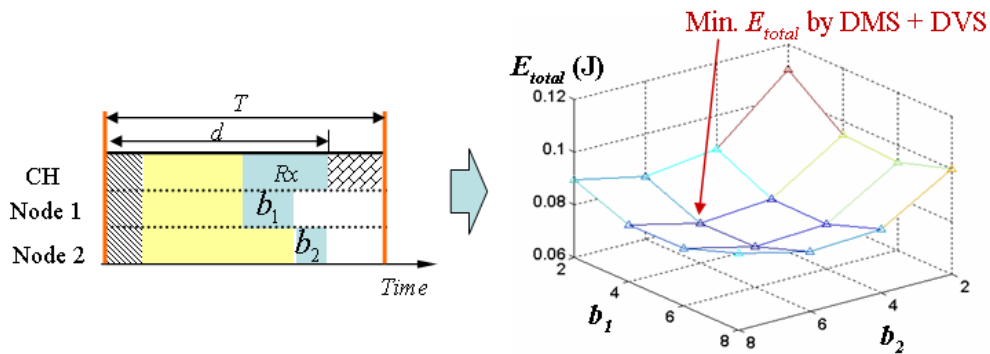


Figure 18: Energy consumption for a 2-node case

In a sensor network with more sensor nodes, the DTA was used to compute the optimal modulation level for every sensor node. Figure 19 shows the energy saving ratio for using the reconfiguration techniques (scenario 2 and scenario 3) with respect to non-reconfigurable scheme (scenario 1), where the energy saving ratio was calculated by:

$$\text{Energy Saving Ratio} = 1 - \frac{E_{total} \text{ with DVS}}{E_{total} \text{ without DVS + DMS}} \quad (\text{for scenario 2}) \quad (20)$$

$$\text{Energy Saving Ratio} = 1 - \frac{E_{total} \text{ with DVS + DMS}}{E_{total} \text{ without DVS + DMS}} \quad (\text{for scenario 3}) \quad (21)$$

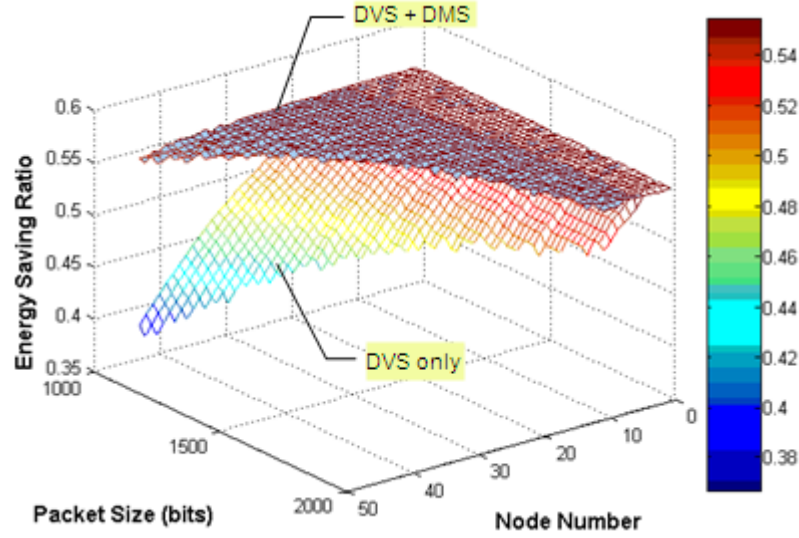


Figure 19: Energy consumption for various node number and packet sizes

Figure 19 shows the energy saving for schemes 2 and 3 for various packet size ( $H$ ) and node number ( $m$ ). With the increment of sensor nodes in the cluster, the average processing time for every sensor node decreased, which increased the energy consumption of the sensor nodes, so the energy efficiency of using DVS technique alone decreased from 55% to 38%. By combining the DMS technique with the DVS technique to allocate the time resource, the increment of computation energy could be reduced by reallocating time resource from the transmission time to the computation time. This time reallocation process increased the communication energy, but resultant energy consumption decreased when the communication distance  $r$  was short. A 22% of energy efficiency improvement was achieved by using DMS with DVS compared to the scenario where only DVS was used.



Similar to the increasing node number, increasing the communication workload reduced the available time for computation, so using DVS alone resulted in the decrease of energy efficiency. With reallocation of time resource, the increased communication time due to the increased communication workload could be shortened, thus prolonging the computation time and correspondingly decreasing the computation energy. By incorporating DMS with DVS, a 52% of energy savings was achieved in high communication task, and the energy efficiency of using DMS with DMS was improved 22% compared to only the DVS technique was used.

The computation efficiency of using the developed DTA algorithm was also investigated to estimate the computation time of finding the solution of the optimization. The total computation time for various number of sensor nodes is shown in Figure 20. The simulation result showed that the optimal solution could be realistically implemented on the cluster head.

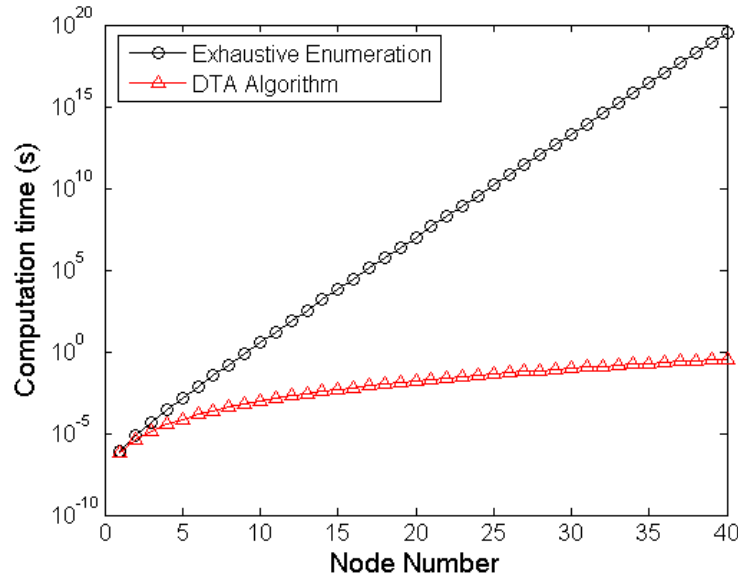


Figure 20: Computation time of the Dynamic Time Allocation algorithm

### 3.2 Network-Level Reconfiguration

Since current state-of-the-art sensor node platforms still cannot meet the demand for high energy-efficiency, particularly in computation-intensive applications such as image processing or vibration analysis, a WSN required a recharging service to recharge the energy-depleted sensor nodes. The entire system could thus be called a Rechargeable Wireless Sensor Network (RWSN). Hence, when a sensor node stopped functioning due to discharge of the limited battery energy available, its battery could be recharged by the recharging service to restore the sensor node to a functional level.

To realize a functional RWSN, the associated maintenance cost needed to be minimized as it ultimately determined the acceptability of the RWSN. The cost was related to the recharging rate (the number of recharging energy-depleted sensor nodes per unit time), which must be minimized. Intelligent node activation was an approach to achieving this objective by dynamically controlling node activities to conserve energy at the sensor node level. It involved redundant deployment of sensor nodes to allow a sensor node to go into sleep mode without degrading network performance. This reduced the overall energy consumption of the network by taking redundant nodes off line and scheduling active/sleep states of the sensor nodes [37].

Traditional scheduling algorithms based on a battery-powered scenario were not suitable for RWSN because these algorithms did not consider the scenario of recharging the sensor nodes. Thus, a new algorithm was required for solving the node activation problem of a RWSN. A major challenge in developing such an algorithm was to tackle the dynamic discharging and recharging processes during the network operation. A dynamic discharging process was necessitated by the random occurrence of events of

interest, which affected the energy consumption in data processing and data communication. The random occurrence of objects in a surveillance sensor network that resulted in the temporal and spatial variation of energy consumption of sensor nodes was one such event. An unpredictable recharging service, where the waiting time for the energy-deployed sensor nodes varied depending on the progress of the recharging service was another. Such applications motivated the development of an analytical framework that captured the stochastic nature of RWSN network operations.

In the following sections, the background of RWSN and related research was first presented. Mathematical formulation of the problem was then developed. Finally, the effectiveness of the developed algorithm was demonstrated.

### **3.2.1 Background**

The realization of a RWSN was tied to the recharging service to sustain the network operation. When the battery voltage of a sensor node dropped below a threshold level due to the sensing operation and data communications, the sensor node stopped the sensing operation and transitions from the *active state* to the *passive state*, waiting for the recharging service. After recharging for a time until the completion of the recharging service, the sensor node went into the *ready state* and could be activated at any time to rejoin the network operation. Thus, every sensor node in a RWSN operated among the three node states as shown in Figure 21, and ideally, the network should be able to operate continually as long as the recharging service was functional.

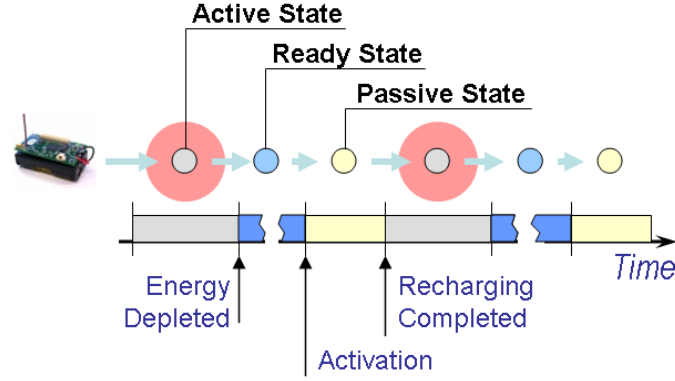


Figure 21: Three node states of sensor nodes in RWSN

The network performance of a RWSN, such as area coverage, network connectivity, or network detectability of a moving target, was determined by the number of sensor nodes in the active state, which varied with time due to the stochastic discharging and recharging time. Sufficient recharging service had to be provided in order to achieve the required time-average network performance. In this paper, *area coverage*, the fraction of the geographical area covered by one or more sensor nodes, was used as the performance metric of the network since it was widely used in WSN [38, 39]. However, the other network performances could also be applied by changing the utility function. Assuming every sensor node had a disk shaped sensing area with same sensing range  $r$ , a sensor node could only detect events that happened within its sensing range. Assuming sensor nodes were distributed uniformly and independently in the sensor field [39], the utility function for calculating area coverage  $U$  was:

$$U(d) = 1 - e^{-d \cdot \tau \cdot r^2} \quad (22)$$

where  $d$  is the active node density (number of active sensor nodes per unit area) and the time-average area coverage  $\bar{U}$  was:

$$\bar{U} = \lim_{t \rightarrow \infty} \frac{1}{t} \int_0^t U(d) dt \quad (23)$$

The area coverage as a function of  $d$  was a monotonically increasing concave function as shown in Figure 22. The purpose of intelligent node activation was to influence the distribution of  $d$  with respect to time by a sequence of activation decisions, so the time-average area coverage could be maximized.

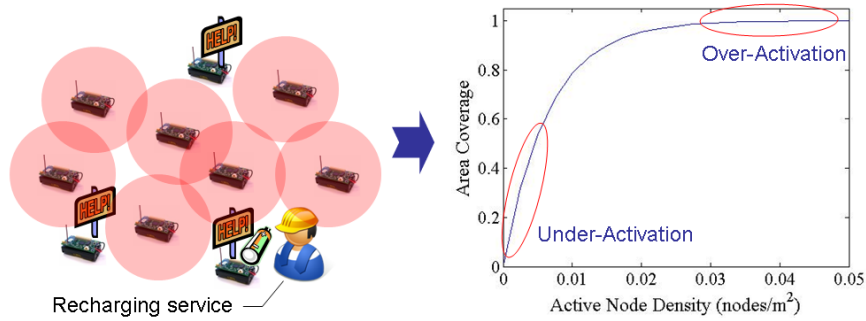


Figure 22: Recharging scheme and area coverage w.r.t. active node density ( $r = 7$  m)

However, over-activation of sensor nodes increased a short-term marginal increment of area coverage but lead to less active sensor nodes in a later time, which resulted in a poor time-average area coverage. Conversely, under-activation directly resulted in poor area coverage. Deriving an activation policy to prevent over-activation or under-activation was the critical problem for the efficient use of RWSN.

### 3.2.2 Literature Review

The scenario of RWSN could represent traditional maintenance service, where the energy-depleted sensor nodes were recharged by technicians. The RWSN could also represent several scenarios for inaccessible WSNs, where the recharging services were used to sustain the network operation. For instance, in [40], one or multiple mobile robots were placed in the sensor field. These mobile robots could move to the location

of every sensor node to recharge the sensor nodes through inductive coupling or direct electrical connection. In [41, 42], some mobile sensor nodes with energy-harvesting capability could deliver energy to the stationary sensor nodes to perform the recharging service. Intelligent node activation for these RWSN scenarios was important in reducing the burden of the recharging service.

The node activation problem for RWSN was first addressed by Kar in 2005 [43]. In this paper, a simple Threshold Activation Policy (TAP) was proposed instead of directly formulating a stochastic decision process. In the TAP algorithm, by assigning a parameter  $s$ , a ready node was activated only when the number of active nodes is below  $s$ ; otherwise, the node stayed at the ready state until any active node depletes its energy. The advantage of using TAP was that the network operation could be modeled as a closed queueing network, and the static analysis approach for a queueing model could be used to derive the optimal threshold value. In [44], the problem was modeled as a closed two queue system where the node activation was derived by the optimal control of admission to a station. However, a mathematical model based on the stochastic decision process was required to gain an insight into the node activation problem and provide an analytical framework for further related problems.

The operation of the rechargeable sensor network utilizing the TAP algorithm is illustrated in Figure 23, there were two stations in tandem in the queueing network. The first station represented the discharging process in which at most  $s$  active nodes were allowed to stay; otherwise, the remaining nodes had to queue in the ready state. The second station represented the recharging process with infinite capacity. The nodes in the active state drained out their energy reserve immediately enter this station waiting

for recharging service. After the recharging service, the nodes returned the first station and repeated the same cycle.

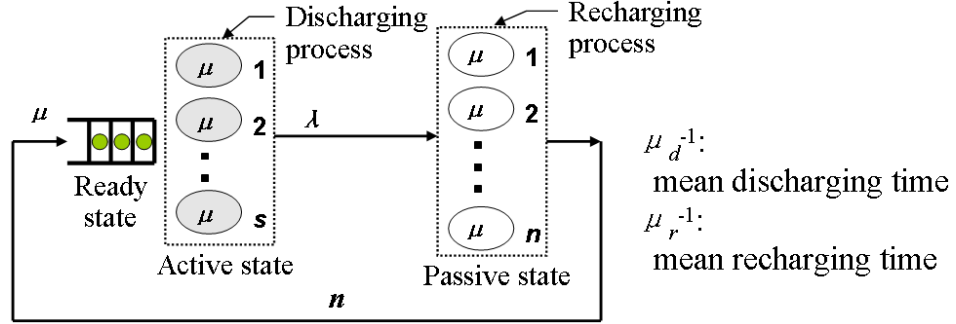


Figure 23: Queueing network model

Under the assumption of exponentially distributed discharging time and recharging time with means  $\mu_d^{-1}$  and  $\mu_r^{-1}$ , the analysis approach for queueing model could be used to derive the equilibrium probability of the model. The analysis was preceded in the following way. First, depending on the number of nodes in the two stations, the system could be defined in the state of  $(n_1, n_2)$ , where  $n_1$  was the number of nodes in the first station and  $n_2$  was the number of nodes in the second station. For the *independent sensor lifetime* where discharging and recharging times of all nodes were mutually independent, when  $n_1 = j$ , the arrival rate of the first station,  $\mu_j$ , could be expressed as:

$$\mu_j = (n - j) \cdot \mu_r, \quad j = 0, 1, \dots, n \quad (24)$$

The departure rate of the first station,  $\lambda_j$ , was expressed as:

$$\lambda_j = \begin{cases} j \cdot \mu_d, & j = 1, 2, \dots, s \\ s \cdot \mu_d, & j = s+1, s+2, \dots, n \end{cases} \quad (25)$$

Based on Equations 24 and 25, the relation between system states are illustrated in Figure 24. In the figure, each circle represented the system state  $(n_1 = j, n_2 = n - j)$ . The arrows connecting two system states were the transition rate between states. The dotted

line separated the system states into the condition that no ready nodes queued in the first station (left side) and ready nodes queued in the first station (right side).

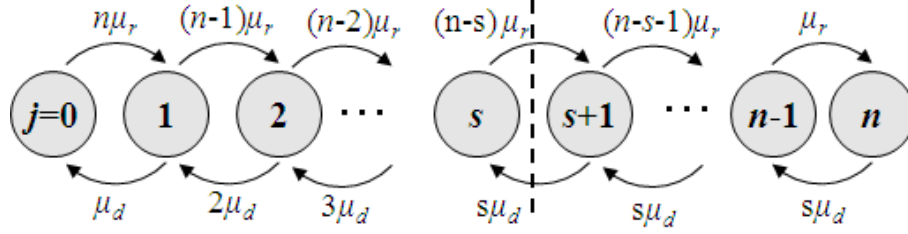


Figure 24: Transition process of the queueing model

The equilibrium probabilities for system state ( $n_1 = j, n_2 = n - j$ ),  $P_j$ , could be derived from a set of balance equations as shown in Table 4.

Table 4: Balance equations of the queueing model

System State	Flow-Out = Flow-In
$j = 0$	$P_0 \cdot n \mu_r = P_1 \cdot \mu_d$
$1 \leq j \leq s-1$	$P_j \cdot [(n-j) \cdot \mu_r + j \mu_d] = P_{j-1} \cdot (n-j+1) \cdot \mu_r + P_{j+1} \cdot (j+1) \cdot \mu_d$
$j = s$	$P_s \cdot [(n-s) \cdot \mu_r + s \mu_d] = P_{s-1} \cdot (n-s+1) \cdot \mu_r + P_{s+1} \cdot s \mu_d$
$s+1 \leq j \leq n-1$	$P_j \cdot [(n-j) \cdot \mu_r + s \mu_d] = P_{j-1} \cdot (n-j+1) \cdot \mu_r + P_{j+1} \cdot s \mu_d$
$j = n$	$P_n \cdot s \mu_d = P_{n-1} \cdot \mu_r$

By introducing the normalized condition,  $\sum_{j=0}^n P_j(n) = 1$ , the equilibrium probability for each system state could be obtained as:

$$P_j = \begin{cases} \binom{n}{j} a^j P_0, & j = 1, 2, \dots, s-1 \\ \frac{n!}{(n-j)! s! s^{j-s}} a^j P_0, & j = s, s+1, \dots, n \end{cases} \quad (26)$$

where  $a = \mu_r / \mu_d$  and  $P_0$  is given by:

$$P_0 = \left[ \sum_{k=0}^{s-1} \binom{n}{k} a^k + \sum_{k=s}^n \frac{n!}{(n-k)! s! s^{k-s}} a^k \right]^{-1} \quad (27)$$

The time-average area coverage,  $\bar{U}$ , was thus calculated from:



$$\bar{U} = \sum_{j=1}^s U(j) \cdot P_j + \sum_{j=s+1}^n U(s) \cdot P_j \quad (28)$$

By selecting appropriate threshold value,  $s$ , that maximizes  $\bar{U}$ , a near-optimal time-average area coverage could be obtained. As for the *correlated sensor lifetime* where the discharging (recharging) times of all nodes entering the active (passive) state at the same time was the same, the time-average area coverage could also be derived by using a variant of the queueing model. Figure 25 illustrates the results computed from the threshold activation policy for the independent and correlated sensor lifetime.

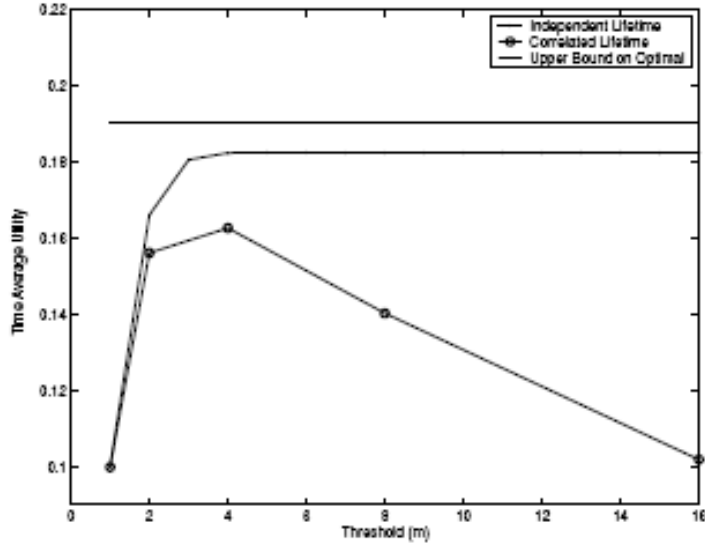


Figure 25: Time-average area coverage for threshold activation policy [43]

The theoretically upper bound of  $\bar{U}$  was  $U(\frac{n}{1+a^{-1}})$  and the threshold activation policy was proved to achieve at least  $\frac{3}{4}$  of the theoretical upper bound [43]. The simple characteristic of TAP algorithm made it easy to be implemented on nodes, and the algorithm required the nodes only to keep track of the node states in its immediate neighborhood.

### 3.2.3 Semi-Markov Decision Process

The main contribution of this technique was the mathematical formulation of the intelligent node activation problem. Two assumptions were made in the model for analytical tractability.

(1) *Markovian property*: The future network state depended only upon the present state and the selected activation decision, without influence by the previous history. This was an important simplifying assumption, which reduced the complexity of planning decisions.

(2) *Exponential distribution of service time*: The discharging and recharging times of any sensor node were assumed exponentially distributed with means  $\mu_d^{-1}$  and  $\mu_r^{-1}$ . The exponential distribution enabled the occurrence of the event to exhibit the Markov property, so the remaining time to the next event was always independent of the previous elapsed time.

The optimal activation decisions under these assumptions depended only on the number of sensor nodes in different node states. Without the assumptions, the network operation would be very difficult to analyze, and required more exchange of network information at the cost of increased communication overhead. Under the two assumptions, the operation of a RWSN could be cast as a Semi-Markov Decision Process (SMDP). The optimal activation decisions could be analytically derived by building the model for SMDP.

### 3.2.3.1 Model Definition

Some basic terms of the SMDP related to the problem were first defined. The *network state*, which was used to represent the network status, was defined as the distribution of sensor nodes in the three node states. The network state was denoted as  $s_i = (n_r, n_a, n_p)$ , where  $n_r$ ,  $n_a$ , and  $n_p$  were the number of sensor nodes in ready, active, and passive state. The sum of  $n_r$ ,  $n_a$ , and  $n_p$  was equal to the total number of sensor nodes,  $n$ . Accordingly, there were  $(n+1) \cdot (n+2) / 2$  states for an  $n$ -node sensor network. For example, a 3-node sensor network had 10 network states, which are listed in Table 5.

Table 5: Network States for a 3-node Sensor Network

States	$n_r$	$n_a$	$n_p$
$s_1$	0	0	3
$s_2$	0	1	2
$s_3$	0	2	1
$s_4$	0	3	0
$s_5$	1	0	2
$s_6$	1	1	1
$s_7$	1	2	0
$s_8$	2	0	1
$s_9$	2	1	0
$s_{10}$	3	0	0

The *action* represented the activation decision at each network state in our problem. The purpose of taking actions in a decision process was to influence the proceeding network states in order to maximize the time-average area coverage. The actions were denoted as  $a_m$ , where  $m$  represented the number of ready nodes being activated at a specific network state. For network state  $s_i = (n_r, n_a, n_p)$ ,  $m$  could be a value between 0 and  $n_r$ . The *policy*, denoted as  $\varphi$ , determines the action chosen in every network state. The policy for a network with  $x$  network states was a  $x$ -tuple. Each element of the  $x$ -tuple specified the action to be selected in each network state according to the policy  $\varphi$ .

For a 3-node sensor network, when the policy  $\varphi = (a_0, a_0, a_0, a_1, a_0, a_1, a_0, a_1, a_2, a_2)$  was adopted, no node would be activated in network states  $s_1, s_2, s_3, s_5, s_7$ , only one node would be activated in network states  $s_4, s_6, s_8$ , and two nodes would be activated in network states  $s_9, s_{10}$ .

### 3.2.3.2 Transition Properties

When an action was selected in a network state, the network undergone a transition process with specific duration (*transition time*), area coverage (*transition reward*), and then jumped to another network state with specific probability (*transition probability*). These transition properties constituted the theoretical model of a SMDP problem, so it was critical to model the transition process for the derivation of these transition properties. When action  $a_m$  was adopted in network state  $s_i = (n_r, n_a, n_p)$ , the network immediately changed to an *intermediate network state*  $s_i' = (n_r - m, n_a + m, n_p)$  and started a transition process as shown in Figure 26.

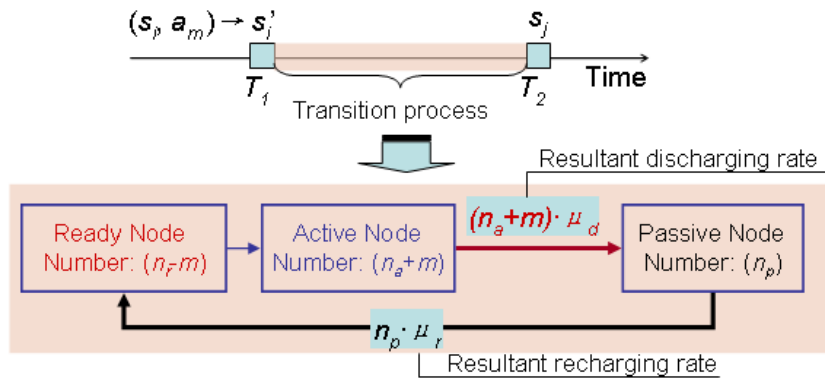


Figure 26: The network state, selected action, and sequential transition process

Under the assumption of the exponential distribution of the mean discharging rate  $\mu_d$  and mean recharging rate  $\mu_r$ , the *resultant discharging rate* of active nodes entering

the passive state was  $(n_a+m) \cdot \mu_d$ , and the *resultant recharging rate* of passive nodes entering the ready state was  $n_p \cdot \mu_r$ . Primarily, these two events caused the network to change state and terminate the transition process. When an active node entered the passive state, the network jumped from the intermediate network state  $s_i'$  to state  $s_j = (n_r-m, n_a+m-1, n_p+1)$ ; when a passive node entered the ready state, the network jumped from the intermediate network state  $s_i'$  to network state  $s_j = (n_r-m+1, n_a+m, n_p-1)$ . Assuming the possibility that multiple events happened at the same time was negligible,  $s_j$  could only be the above two network states. The transition properties for each network state-action pair were thus computed based on this transition process.

*Transition probability*,  $p(s_i, a_m, s_j)$ , was the probability that the network jumped to the next network state  $s_j$  when action  $a_m$  was selected at the current network state  $s_i$ . The  $s_j$  could only be  $(n_r-m, n_a+m-1, n_p+1)$  and  $(n_r+1, n_a, n_p-1)$  depending on which event happens first in the network: an active node entering the passive state or a passive node entering the ready state. The transition probability to these two network states were the fraction of the resultant discharging rate or the resultant recharging rate to the sum of the two resultant rates, and the transition probabilities to the other network states were zero. Equation 29 mathematically expressed the transition probabilities for all network states as:

$$p(s_i, a_m, s_j) = \begin{cases} \frac{(n_a + m) \cdot \mu_d}{n_p \cdot \mu_r + (n_a + m) \cdot \mu_d} & \text{for } s_j = (n_r - m, n_a + m - 1, n_p + 1) \\ \frac{n_p \cdot \mu_r}{n_p \cdot \mu_r + (n_a + m) \cdot \mu_d} & \text{for } s_j = (n_r - m + 1, n_a + m, n_p - 1) \\ 0 & \text{for other networkstates} \end{cases} \quad (29)$$

The derivation of Equation 29 was as follows. We denoted  $E = E_a$  to represent the event that an active node first entered the passive state within the transition process and  $E = E_p$  represented the event that a passive node first entered the ready state during the transition process. Assuming  $U = \min\{E_a, E_p\}$ , the probability that  $\{E = E_a \text{ and } U > t\}$  was equal to:

$$\begin{aligned}
\Pr\{E = E_a, U > t\} &= \Pr\{t < E_a < E_p\} \\
&= \iint_{t < x_a < x_p} (n_a + m)\mu_d e^{-(n_a+m)\mu_d x_a} n_p \mu_r e^{-n_p \mu_r x_p} \\
&= \int_t^\infty e^{-n_p \mu_r x_a} (n_a + m)\mu_d e^{-(n_a+m)\mu_d x_a} dx_a \\
&= \frac{(n_a + m)\mu_d}{(n_a + m)\mu_d + n_p \mu_r} \int_t^\infty ((n_a + m)\mu_d + n_p \mu_r) e^{-((n_a+m)\mu_d + n_p \mu_r) x_a} dx_a \\
&= \frac{(n_a + m)\mu_d}{(n_a + m)\mu_d + n_p \mu_r} e^{-((n_a+m)\mu_d + n_p \mu_r) t}
\end{aligned} \tag{30}$$

The transition probability  $p(s_i, a_m, s_j)$  for  $s_j = (n_r - m, n_a + m - 1, n_p + 1)$  was:

$$\Pr\{E = E_a\} = \Pr\{E = E_a, U > 0\} = \frac{(n_a + m)\mu_d}{(n_a + m)\mu_d + n_p \mu_r} \tag{31}$$

The transition probability  $p(s_i, a_m, s_j)$  for  $s_j = (n_r + 1, n_a, n_p - 1)$  was:

$$\Pr\{E = E_p\} = 1 - \Pr\{E = E_a\} = \frac{n_p \mu_r}{(n_a + m)\mu_d + n_p \mu_r} \tag{32}$$

*Transition time*,  $t(s_i, a_m, s_j)$ , was the duration from the current network state  $s_i$  to the next network state  $s_j$  given action  $a_m$  was chosen at  $s_i$ . Since the transition time was a random variable due to the stochastic discharging and recharging process, the value of the transition time was determined by the expected value of  $t(s_i, a_m, s_j)$ . Because the resultant recharging time and resultant discharging time were distributed exponentially

with means of  $(n_p \cdot \mu_r)^{-1}$  and  $((n_a + m) \cdot \mu_d)^{-1}$ , the probability that the network changed the network state at time  $t$  was calculated as:

$$\begin{aligned} f(t | s_i, a_m) \\ = ((n_a + m) \cdot \mu_d + n_p \cdot \mu_r) \cdot e^{-((n_a + m) \cdot \mu_d + n_p \cdot \mu_r) \cdot t} \end{aligned} \quad (33)$$

To derive the probability density function,  $f(t | s_i, a_m)$ , we first obtained the cumulative distribution function via

$$\begin{aligned} 1 - \Pr\{U > t\} &= 1 - \Pr\{E = E_a, U > t\} - \Pr\{E = E_p, U > t\} \\ &= 1 - e^{-((n_a + m) \mu_d + n_p \mu_r) t} \left( \frac{(n_a + m) \mu_d}{(n_a + m) \mu_d + n_p \mu_r} + \frac{n_p \mu_r}{(n_a + m) \mu_d + n_p \mu_r} \right) \\ &= 1 - e^{-((n_a + m) \mu_d + n_p \mu_r) t} \end{aligned} \quad (34)$$

The probability density function (Equation 33) could then be derived by taking the first derivative of the above cumulative distribution function.

The expected value of  $t(s_i, a_m, s_j)$  over all network states was calculated as:

$$\begin{aligned} t(s_i, a_m, s_j) \\ = \int_0^{\infty} t \cdot f(t | s_i, a_m) dt = \frac{1}{(n_a + m) \cdot \mu_d + n_p \cdot \mu_r} \end{aligned} \quad (35)$$

*Transition reward* represented the area coverage in our case since area coverage was used as the performance metric of the network. According to Equation 23, the value of the area coverage was expressed as:

$$U(d = N_a / A) = 1 - e^{-d \cdot \pi \cdot r^2} \quad (36)$$

where  $A$  is the total area of the sensor field and  $N_a$  is the number of active nodes. The transition reward,  $r(s_i, a_m, s_j)$ , represented the area coverage in the transition process when the network was going from network state  $s_i$  to  $s_j$  under the influence of action  $a_m$ . Because the system stayed at the intermediate network state during the whole transition

process, the transition reward was completely governed by the active node numbers in the intermediate network state, and was calculated as:

$$r(s_i, a_m, s_j) = U\left(\frac{n_a + m}{A}\right) \quad (37)$$

In the next section, the derived transition properties were embedded into the SMDP model to obtain the optimal policy that maximized the time-average area coverage.

### 3.2.3.3 Solution Formulation

The objective of formulating the SMDP was to find the optimal policy,  $\varphi^*$ , which maximized the time-average reward (area coverage) as expressed by:

$$\lim_{t \rightarrow \infty} \frac{1}{t} E \left[ \int_{x=0}^t U(d) dx \right] \quad (38)$$

where  $d$  is the active node density that varies with time. This average utility problem could be solved by using the discounted utility problem as the discounted factor,  $e^{-\alpha x}$ , approached unity. Specifically, considered the problem of maximizing:

$$\lim_{t \rightarrow \infty} E \left[ \int_{x=0}^t e^{-\alpha x} \cdot U(d) dx \right] \quad (39)$$

where  $\alpha$  is the discounting coefficient. The policy that optimized the total discounted reward in Equation 39 is also the optimal policy for the problem of Equation 38 when the discounted coefficient  $\alpha$  approached zero [45]. The policies for SMDP were evaluated with respect to this expected total discounted reward in order to avoid an unbounded value function problem when using the Bellman equation. The Bellman equation used the recurrent relationship of state to yield optimal solutions to SMDP problems. In the Bellman equation, associated with every network state, there existed a scalar quantity for a given policy. Each scalar quantity, called a *value function*, was the



expected total discounted reward starting from a given network state along the infinite time trajectory. These quantities formed a value function vector, which needed to be maximized by choosing an optimal policy.

The basic recurrence concept of the Bellman equation was illustrated in Figure 27 [46, 47], where  $J_\varphi(s_i)$  denotes the value function of state  $s_i$  under policy  $\varphi$ . Assuming the next network state was  $s_j$ , the transition time  $t(s_i, \varphi(s_i), s_j)$  and the transition reward  $r(s_i, \varphi(s_i), s_j)$  could be calculated from the previous section. According to the definition of the value function,  $J_\varphi(s_i)$  was equal to the total discounted reward earned during the one-step transition from  $s_i$  to  $s_j$  plus the value function of the network state  $s_j$ . Such a recurrence relationship was mathematically expressed as:

$$J_\varphi(s_i) = R(s_i, \varphi(s_i), s_j) + e^{-\alpha t(s_i, \varphi(s_i), s_j)} \cdot J_\varphi(s_j) \quad (40)$$

where  $R(s_i, \varphi(s_i), s_j)$  is the total discounted reward earned during the one-step transition process. The value of  $R(s_i, \varphi(s_i), s_j)$  was the expected value of the total discounted reward, which was calculated from:

$$R(s_i, \varphi(s_i), s_j) = \int_{x=0}^{\infty} \left[ \int_{t=0}^x e^{-\alpha t} \cdot r(s_i, \varphi(s_i), s_j) dt \right] f(x | s_i, \varphi(s_i)) dx \quad (41)$$

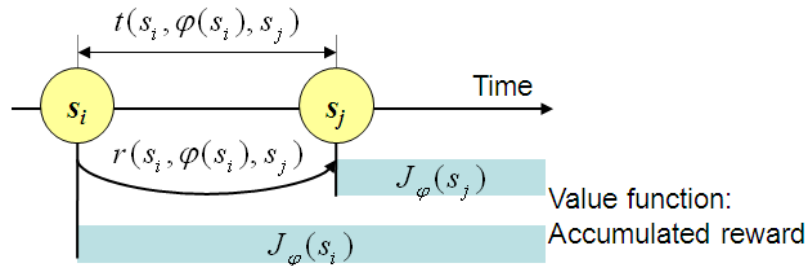


Figure 27: Recurrence relation of the network states and associated value functions

If the action specified by the policy  $\varphi$  at state  $s_i$ ,  $\varphi(s_i)$ , was  $a_m$ , then Equation 41 could be further simplified to:

$$R(s_i, \varphi(s_i), s_j) = \frac{r(s_i, \varphi(s_i), s_j)}{\alpha + [(n_a + m) \cdot \mu_d + n_p \cdot \mu_r]} \quad (42)$$

Furthermore, since  $s_j$  could be any state, the expectation of  $J_\varphi(s_i)$  over all network states was used in Equation 40 by introducing the transition probability  $p(s_i, \varphi(s_i), s_j)$ :

$$\begin{aligned} J_\varphi(s_i) &= \sum_{s_j \in S} p(s_i, \varphi(s_i), s_j) [R(s_i, \varphi(s_i), s_j) + e^{-\alpha \cdot t(s_i, \varphi(s_i), s_j)} \cdot J_\varphi(s_j)] \\ &= R(s_i, \varphi(s_i)) + \sum_{s_j \in S} p(s_i, \varphi(s_i), s_j) \cdot e^{-\alpha \cdot t(s_i, \varphi(s_i), s_j)} \cdot J_\varphi(s_j) \end{aligned} \quad (43)$$

where  $R(s_i, \varphi(s_i))$  is the expected value of  $R(s_i, \varphi(s_i), s_j)$  over the set of all network states,  $S$ . Equation 43 was the final form of the Bellman equation for one of the network states.

The Bellman equation was therefore a system of linear equations in which the unknowns were the elements of the value function associated with the given policy.

By solving the Bellman equation, the value function vector associated with a given policy was obtained. The optimal policy was found by enumerating every possible policy and choosing the policy that produces the maximum value function. However, such an exhaustive enumeration was not an attractive proposition from the computational point of view. Hence, the value iteration method, a computation-efficient algorithm, was utilized in our study to solve the Bellman equation.

### 3.2.3.4 Value Iteration Algorithm

The value iteration algorithm was chosen to compute the optimal policy due to its computation efficiency and simple program structure. The value iteration algorithm

used the Bellman optimality equation, which was modified from the Bellman equation, to avoid the necessity of solving the system of equations. The Bellman optimality equation used for the value iteration was expressed as:

$$\begin{aligned} J^*(s_i) &= \max_{a_m \in A(s_i)} [R(s_i, a_m) + \sum_{s_j \in S} e^{-\alpha t(s_i, a_m, s_j)} \cdot p(s_i, a_m, s_j) \cdot J^*(s_j)] \end{aligned} \quad (44)$$

where  $A(s_i)$  is the set of available actions in network state  $s_i$  and  $J^*$  terms are the optimal value functions computed from the optimal policy. The algorithm needed for solving the Bellman optimality equation was given below:

Step 1: Set  $k = 1$  and select an arbitrary vector  $J^1$ . Specify  $\varepsilon > 0$ .

Step 2: For each  $s_i \in S$ , compute Equation 45, i.e., find the action that maximizes the updated value function:

$$\begin{aligned} J^{k+1}(s_i) \leftarrow & \max_{a_m \in A(s_i)} [R(s_i, a_m) + \sum_{s_j \in S} e^{-\alpha t(s_i, a_m, s_j)} \cdot p(s_i, a_m, s_j) \cdot J^k(s_j)] \end{aligned} \quad (45)$$

Step 3: If  $\text{span}(J^{k+1} - J^k) < \varepsilon$  (which will be discussed later) go to Step 4; Otherwise increase  $k$  by 1 and go back to Step 2.

Step 4: For each  $s_i \in S$ , choose the  $\varepsilon$ -optimal policy,  $\beta$ , according to Equation 46 and stop.

$$\begin{aligned} \beta(s_i) \in & \arg \max_{a_m \in A(s_i)} [R(s_i, a_m) + \sum_{s_j \in S} e^{-\alpha t(s_i, a_m, s_j)} \cdot p(s_i, a_m, s_j) \cdot J^k(s_j)] \end{aligned} \quad (46)$$

The value iteration algorithm initiated from a random selected value function vector  $J^1$ . During the iteration  $k$ , the Bellman optimality equation in Step 2 produced an updated value function vector  $J^{k+1}$  and an improved policy  $d^{k+1}$  by selecting the action

$a_m$  that maximized the value function. As the iteration number increased, the obtained policy  $d$  approached the optimal policy and the value function converged to the optimal value function. The termination mechanism in Step 3 used the *span* [48]. Given a vector  $\vec{x}$ , the span of  $\vec{x}$  is defined as:

$$span(\vec{x}) = \max_i x(i) - \min_i x(i) \quad (47)$$

With the increment of the iteration number, the span of the difference vector ( $J^{k+1} - J^k$ ) kept getting smaller. The parameter  $\varepsilon$  was used to set the stopping criteria. The iteration terminated when the span of the difference vector for two consecutive value function vectors was smaller than  $\varepsilon$ . Hence, for a given positive value of  $\varepsilon$ , the algorithm terminated in a finite number of steps. At the end of the algorithm, a near-optimal policy could be produced which tries to maximize the time-average area coverage of the network. The smaller the value of  $\varepsilon$ , the closer the obtained policies were to the optimal policy, but it also resulted in a longer computational time to produce the near-optimal policy.

The SMDP algorithm for intelligent node activation was based on a centralized scheme, where a central sensor node kept track of every sensor node's status and determined the activation of ready nodes according to the optimal policy. Since the sensor nodes changed their node states only when they deplete their energy or finish recharging, a constant information exchange between the network nodes could be avoided. This minimized the communication energy overhead. A simulation of the intelligent node activation was conducted to test the effectiveness of the proposed SMDP algorithm.

### 3.2.4 Simulation Model and Results

A surveillance application was used to evaluate the SMDP algorithm. Area coverage was an important performance metric for a surveillance system. The sensor nodes were assumed to be deployed uniformly and independently on a sensor field with node density  $d_n = 0.04$  nodes/m<sup>2</sup>. This was the node density used by warehouse or residential monitoring scenarios. Every sensor node was equipped with multiple sensors to increase the capability in classifying the targets. A magnetometer, an infrared sensor, and an acoustic sensor with sensing ranges of 7, 12, and 50 m, respectively were included [49]. The sensing range for every sensor node was assumed to be 7 m, which was the shortest sensing range of the three sensors. Two different correlation models for the sensor nodes were considered:

*Independent sensor model:* The discharging and recharging times of all sensor nodes were mutually independent.

*Correlated sensor model:* The sensor nodes entered the active (passive) state at the same time and had the same discharging (recharging) time; otherwise, the discharging and recharging times of the sensor nodes were mutually independent to each other.

The two sensor models were used to represent different realistic RWSN environments. If the local computation and the resulting data transmission was the major energy expenditure of a sensor node, the discharging times were better represented by the independent model since the events were assumed to occur randomly in the sensor field. On the other hand, in the rare event application, when the sensing activity was the major source of energy consumption, the discharging times were better modeled by the correlated model. Similarly, the recharging time was better represented

by the independent model when the recharging service was provided individually and by the correlated model when the recharging service could recharge multiple sensor nodes at the same time.

The effectiveness of the SMDP algorithm was compared with the theoretical upper bound of time-average area coverage and with the scenario where no activation algorithm was used. The theoretical upper bound for a specific recharging and discharging rate was calculated by [43]:

$$U_{upper} = U\left(\frac{d_n}{1 + \mu_d / \mu_r}\right) \quad (48)$$

The scenario without using an activation algorithm suggested that the sensor nodes leaving the passive state were activated immediately. The simulation was conducted to acquire the necessary recharging-to-discharging ratio ( $\mu_r/\mu_d$ ) for various time-average area coverage requirements. Under a specific time-average area coverage requirement, a lower recharging-to-discharging ratio suggested that a lower recharging service was required for the RWSN.

Figure 28 illustrates the results for the independent sensor model. The time-average area coverage with and without using intelligent node activation appeared to be close to each other and the results for both cases were close to the upper-bounded value. This was because the distribution of the sensor nodes entering the active state was evenly distributed in the independent sensor model. The situation of over-activation did not happen during this network operation, thus good energy efficiency was achieved with and without the intelligent node activation.

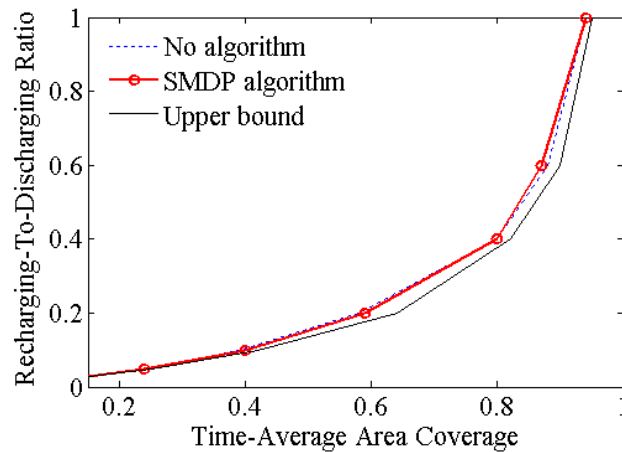


Figure 28: Network performance for the independent sensor model

However, when the sensor model was highly correlated as shown in Figure 29, over-activation of sensor nodes occurred when intelligent node activation was not used. The required recharging-to-discharging ratio had to be increased in order to meet the required time-average area coverage. The utilization of the proposed SMDP significantly reduced the demand for recharging service. For various time-average area coverage requirements, up to 72% of recharging rate was achieved by using SMDP algorithm compared to no activation algorithm was used. The reduced recharging rate greatly decreases the cost, in terms of capital, of maintaining the network.

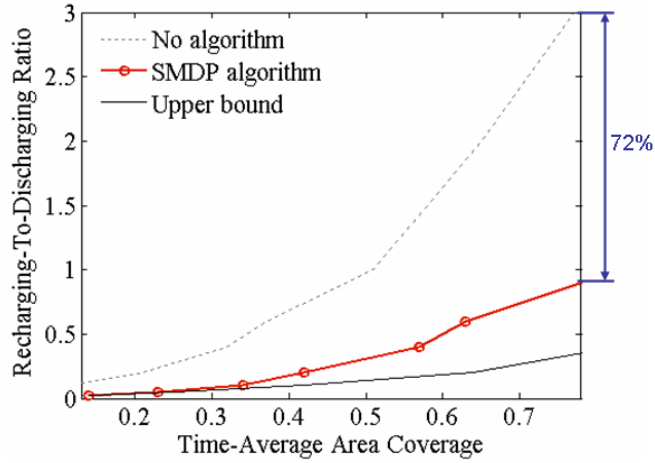


Figure 29: Network performance for the correlated sensor model

In realistic applications, such as surveillance systems or machine monitoring applications, the sensor models tended to be highly correlated because the sensor nodes in the near sensor field had similar probabilities of detecting the same events, and consumed energy at the same rate for the resulting data processing and the data communication operations. The sensor nodes were recharged at the same time very close in time because the recharging services of the sensor nodes were scheduled in a batch due to their geographical proximity. The proposed SMDP algorithm, which performed well in the correlated sensor models, should achieve high energy-efficiency in these applications.



### 3.3 Implementation

This section presents an implementation for the previously proposed energy-efficient data acquisition scheme that enables continued data sampling and on-node data feature extraction, based on the DVS concept. A reservation-based Time Division Multiple Access protocol was employed to allow staggered data transmissions within a sensor cluster. As a result, sensor nodes that were scheduled to transmit their data later in the sequential order could take advantage of the “extra” time allocated to slow down the speed of data processing by lowering the supply voltage, thereby reducing energy consumption. The design of reconfigurable sensor nodes was demonstrated through the integration of a Crossbow Imote2 platform with a customized sensor board. The Imote2 utilized an Intel XScale PXA271 processor with DVS capability. The sensor board, containing a sensor interface and an A/D converter, was designed for high sampling rate applications enabled by Direct Memory Access (DMA) through the Serial Peripheral Interface of the CPU. As a result, concurrent processing of signal sampling and local data computation were achieved for real-time applications.

To evaluate the developed data acquisition scheme, a sensor network was designed that featured autonomous sensor cluster head selection, time synchronization, and dynamic allocation of computation times at the sensor node level. Its performance was comparatively evaluated against a conventional sensor network that employed maximum operating frequency for task execution and transmission using the Carrier Sense Multiple Access (CSMA) protocol. Energy models for these two comparative scenarios were first developed, and simulation results were compared experimentally. It was found that energy reduction of up to 50% could be achieved using the

reconfiguration sensor hardware, which effectively translated into prolonged service life for the sensor network.

### 3.3.1 Network Operation

A self-configuring sensor network system was developed to realize the proposed data acquisition scheme. Figure 30 illustrates the network operation for the implementation of the reconfigurable sensor network.

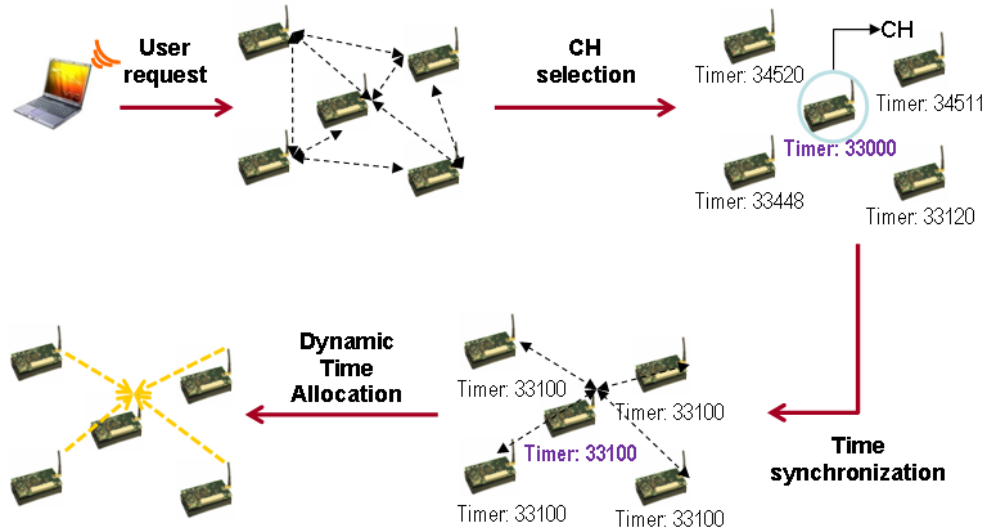


Figure 30: Network initialization and formation

The sensor network was initiated when receiving a request from the base station. At first, a mesh network was formed to select a cluster head (CH). The selected CH then performed time synchronization to align the sampling frames, so every sensor node could perform computation and communication tasks as scheduled in the data acquisition scheme. Afterwards, the CH performed dynamic time allocation to calculate the computation and transmission time ( $\tau_t$  and  $\tau_c$ ) for every sensor node. A sensor network with start topology was then created to begin the data acquisition process.

Because the CH consumed the most energy due to the extra data fusion and data communication, the selection of CH had to be performed periodically in order to distribute the workload to the sensor nodes. The following subsections introduce the important technique and algorithm used in the network operation.

### 3.3.1.1 Cluster Head Selection Algorithm

A distributed algorithm run on individual sensor node without the coordination of a central control unit was developed to select the CH. Unlike the algorithm proposed in [70] that sensor nodes self-elected themselves as a CH with equal probability, the energy level of sensor nodes were considered in our algorithm to select the sensor nodes with higher remaining battery energy as the CH. In the selection mechanism, an energy level index  $\mathfrak{R}$  (0~1) related to the current battery voltage output  $V_{batt}$  was defined as:

$$\mathfrak{R} = \frac{V_{batt} - V_{th}}{V_{max} - V_{th}} \quad (49)$$

where  $V_{th}$  is the minimum battery voltage that can support a normal operation of sensor nodes and  $V_{max}$  it the maximum battery voltage. In the CH selection process, a sensor node self-elected itself as a CH in several attempts  $r$  according to the probability  $P_{elect}$ :

$$P_{elect}(r, \mathfrak{R}) = (w \cdot e^{-x \cdot r} + y) \cdot (z \cdot \mathfrak{R} + \eta) \quad (50)$$

where  $w$ ,  $x$ ,  $y$ , and  $\eta$  are coefficients.  $P_{elect}$  as a function of  $r$  and  $\mathfrak{R}$  increased with  $\mathfrak{R}$ , but decreased with  $r$ . The use of  $r$  prevented the sensor nodes with high remaining energy from continuously competing to each other, which prolonged the total CH selection process. In the CH selection process, at least one attempt ( $r = 1$ ) was performed by every sensor node to elect itself as a CH according to respective  $P_{elect}(r=1,$

$\mathfrak{R}$ ). If a sensor node self-elected itself as the CH, it broadcasted a *CH announcement*, and waited for a period  $t_{CH}$ . If no other sensor nodes also broadcasted the CH announcement within  $t_{CH}$ , the sensor node was selected as the CH; otherwise, the sensor node entered the second attempt ( $r = 2$ ) with a lower self-election probability  $P_{elect}(r=2, \mathfrak{R})$ . A sensor node declared itself as a normal sensor node when it failed in the self-election and heard the CH announcement from other sensor nodes. If a sensor node failed at the self-election but without hearing any CH announcement within  $t_{CH}$  (no sensor node was self-elected as the CH), the sensor node still went to the next attempt and continued to self-election process. The CH selection process lasted until only one sensor node was self-elected as the CH.

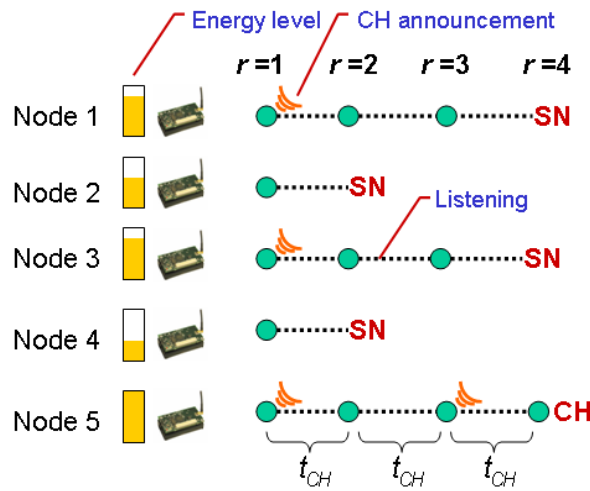


Figure 31: Cluster head selection process

Figure 31 demonstrates the above CH selection process using five sensor nodes (Node 1 ~ Node 5) with different battery energy. In the first attempt of self-election for all sensor nodes, Nodes 2 and 4 with lower  $P_{elect}$  failed in the self-election process. They classified themselves as normal sensor nodes (withdraw from the CH selection process) when they heard the CH announcements broadcasted by Nodes 1, 3, and 5. Nodes 1, 3,

and 5 participated in the second attempt of self-election process. Because no any sensor node succeeded at the self-election process, they all stepped into the third attempt of self-election process in which only Node 5 succeeded in the self-election process. After  $t_{Ch}$ , Node 5 declared itself as the CH, which ended the CH selection process. Consequently, the sensor node with high energy could be selected as CH without exchanging all energy information among the cluster.

### 3.3.1.2 Time Synchronization Protocol

The time synchronization was used in network operation to unify the timer of every sensor node to the timer of CH (global timer). A Flooding Time Synchronization Protocol (FTSP) [50] was adopted that used a single broadcasted message to obtain time synchronization between CH and the other sensor nodes. The FTSP achieved time synchronization utilizing a single radio message time-stamped at both the sender and receiver sides. The broadcasted message contained the 8-byte time-stamped information of the CH. The sensor nodes recorded the local time while receiving the message. Therefore, one broadcast message provided synchronization information (global timer, local timer) for all sensor nodes.

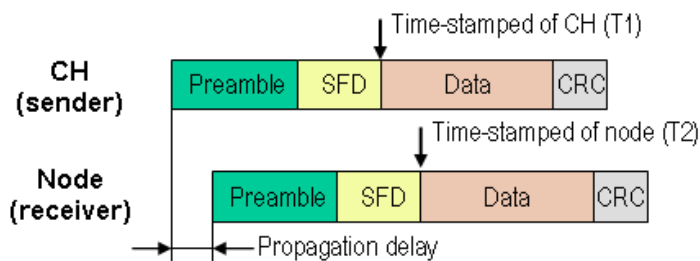


Figure 32: Time synchronization message over the radio

The time synchronization message started with the transmission of preamble bytes, followed by start of frame delimiter field (SFD), followed by the time-stamped data and data used for the estimation of channel condition, and finally ended with CRC bytes. The timer of the CH (T1) and sensor nodes (T2) were stamped at the end of SFD field. There was a time elapsed between transmission of SFD field and reception of SFD field due to the over-the-air propagation and radio hardware propagation. The message layout was illustrated in Figure 32. Since RF propagation time was small in the short-range transmission, its effect could be ignored. The hardware propagation delay was empirically determined. Using T1, T2, and determined propagation delay, the time offset between the global timer and local timer could be calculated by  $T1 - T2 + \text{delay}$ , so the global timer (= local timer + time offset) were available for every sensor node.

The time synchronization was first performed by intensively sending 20 synchronization messages at the initialization stage for fast timer convergence. After that, one time synchronization message was broadcasted at every control sub-frame to rectify the error caused by slightly different frequencies of 13MHz crystal oscillators on sensor nodes for maintaining the synchronization accuracy. The experimental results in [50] showed that the error from such repetitive re-synchronization was below one microsecond, which was precise for sampling frame alignment and the staggered transmission.

### **3.3.1.3 Dynamic Time Allocation**

After the initialization phase (CH selection and time synchronization), the CH determined the sensor node transmission sequence in the data acquisition scheme. The

sensor nodes with higher remaining energy were scheduled at the former sequence to average the remaining energy of sensor nodes. The CH then scheduled the computation time ( $\tau_c$ ) and transmission time ( $\tau_t$ ) for every sensor node according to the time constraint  $d$  and the number of sensor nodes in the cluster  $m$ :

$$\tau_{c,i} = d - (m - i + 1) \cdot \tau_t \quad (51)$$

where  $i$  is the transmission sequence of sensor. The  $\tau_t$ , which depended on the length of the extracted feature, was the same for every sensor node. After receiving the time allocation schedule, every sensor node locally determined the minimum operating frequency  $f$  that satisfied Equation 52 in order to finish the computation task in time.

$$f_i \geq \frac{N}{\tau_{c,i}} = \frac{N}{d - (m - i + 1) \cdot \tau_t} \quad (52)$$

It should be noticed that the maximum operating frequency  $f_{max}$  available for sensor nodes limited the maximum number of sensor nodes  $m_{max}$  that a cluster could accommodate. The  $m_{max}$  was calculated by considering the operating frequency of the Node 1 ( $i=1$ ):

$$\begin{aligned} f_{max} &\geq f_1 \geq \frac{N}{\tau_{c,1}} = \frac{N}{d - m \cdot \tau_t} \\ \Rightarrow m &\leq \frac{1}{\tau_t} \left( d - \frac{N}{f_{max}} \right) = m_{max} \end{aligned} \quad (53)$$

because it possessed the shortest computation time, which required the highest operating frequency.

### 3.3.2 Sensor Node Design

To realize a reconfigurable sensor networks, sensor nodes with DVS reconfigurability were developed to test its feasibility and energy-efficiency. The sensor

node was designed by integrating a Crossbow Imote2 sensor node platform with a customized sensor board. The Imote2 was an advanced sensor node platform specific for application with intensive computation. It had a processor (Intel XScale PXA271) run at 13 – 416MHz with voltage scaling between 0.85 – 1.8V. The large memory capacities, including 256kB SRAM, 32MB SDRAM, and 32MB of FLASH, were sufficient for the implementation of complex signal processing techniques. An integrated low-power 802.15.4 radio (ChipCon CC2420) supported 250kb/s data rate and up to 100 m data communication distance. Figure 33 illustrates the hardware architecture of a sensor node, where the sensor board including A/D converter (ADC) and sensing interface was connected to the Imote2 with external wired sensing elements.

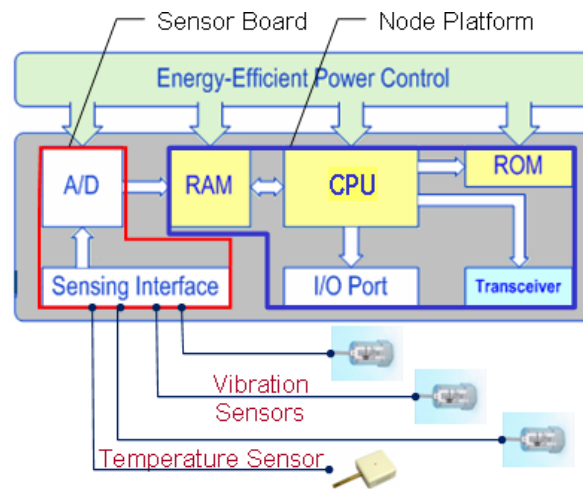


Figure 33: Hardware architecture of the sensor node

The sensor board was designed to provide high sampling rate of signals. The sensor board was chiefly composed of an ADC (Analog Device AD7923) and a DC-DC converter (MAXIM MAX1795). The ADC with 4 channels and 200K sampling rate communicated to the processor through Serial Peripheral Interface (SPI). By utilizing a DMA (Direct Memory Access) controller, the data transmitted from the ADC was



directly stored at the RAM, so the processor could concurrently process the computation task without considering the data acquisition operation. The DC-DC converter, which got a power supply from a 3V output of the processor, provided a 5V output in supporting the ADC and the sensing elements. The DC-DC converter worked for a wide range of operating voltage, so the sensor board could function normally without influenced by the decrease of the battery energy. Figure 34 illustrates the circuit diagram of the designed sensor board.

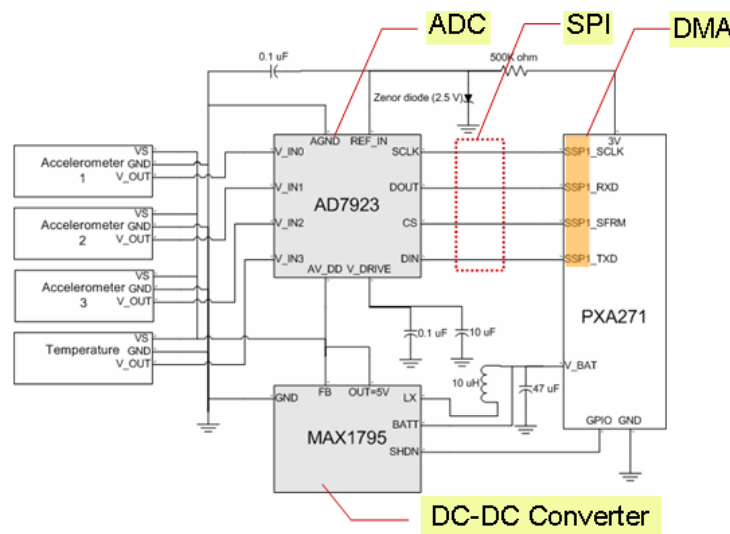


Figure 34: Circuit diagram of the sensor board

### 3.3.3 Experiment

#### 3.3.3.1 Experiment Setup

Assuming a cluster of sensor nodes were deployed on a target system where every sensor node could wireless communicate to each other. Each sensor node continuously monitored the vibration signal and locally performed data processing (requiring  $N = 110 \times 10^6$  machine cycles) based on the Discrete Harmonic Wavelet Packet Transform

(DHWPT) algorithm [51]. The experimental setup for a reconfigurable is illustrated in Figure 35.

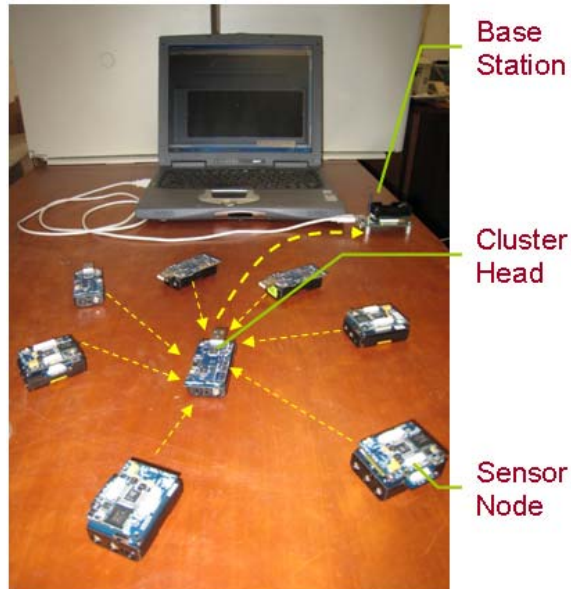


Figure 35: Experimental Setup for a reconfigurable sensor network

The length of the extracted features (energy at each sub-frequency band) was 2.5K bytes, which required 10 milliseconds to transmit. The total time taken for the CH data fusion and data transmission to the base station was 0.45 second, and 50 milliseconds were reserved for control sub-frame. Using a 1-second sampling frame, the time constraint  $d$  for the data computation and data communication was 0.5 second, where the maximum number of sensor nodes in the cluster  $m_{max}$  was 45.

### 3.3.3.2 Energy Measurement

A measurement circuit was designed to measure the power consumption of sensor nodes, as shown in Figure 36. A  $0.25 \Omega$  resistor was in series with the measured sensor node, and the voltage difference between the resistor was amplified by a non-inverting

operational amplifier circuit. The amplified voltage output was measured by an oscilloscope, and the power consumption of the sensor node  $P$  was calculated according to:

$$P = 4.5 \frac{V_o}{R_3} \frac{R1}{R1 + R2} \quad (54)$$

where  $V_o$  is the voltage output read by the oscilloscope.

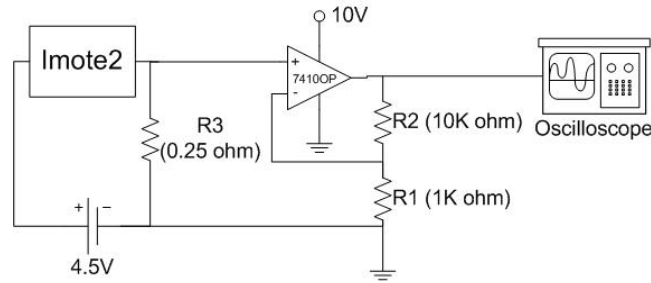


Figure 36: Measurement circuit for power profiling of sensor nodes

### 3.3.3.3 Energy Model

An energy model for the energy consumption of a sensor node within one sampling frame was also developed since it was a time-consuming work in energy measurement. With the energy model, more scenarios can be simulated to see the energy efficiency of the reconfigurable sensor network. The power consumption of a sensor node was first modeled by considering the power consumption contributed from the processor  $P_{comp}$  and from the other circuit components (PLL, oscillator, and I/O interface)  $P_{other}$ . The total power consumption was expressed as:

$$P = P_{comp} + P_{other} = C \cdot V^2 \cdot f + P_{other} \quad (55)$$

The total energy consumption in a sampling frame can be calculated as:

$$\begin{aligned}
E &= P \cdot \tau_c + P_{13\text{MHz}+\text{Radio\_On}} (\tau_t + \tau_{control}) \\
&\quad + P_{13\text{MHz}+\text{Radio\_Off}} (T - \tau_c - \tau_t - \tau_{control}) \\
&= N \cdot C \cdot \left( \frac{N}{K \cdot \tau_c} + \varepsilon \right)^2 + P_{13\text{MHz}+\text{Radio\_On}} (\tau_t + \tau_{control}) \\
&\quad + P_{other} (T - \tau_t - \tau_{control})
\end{aligned} \tag{56}$$

where  $T$  is the length of a sampling frame,  $P_{13\text{MHz}+\text{Radio\_On}}$  is the power consumed at 13MHz with radio on, and  $P_{13\text{MHz}+\text{Radio\_Off}}$  is the power consumed at 13MHz with radio off, which is very close to  $P_{other}$ . Table 6 lists the required hardware parameters used for the above energy calculation.

Table 6: Parameter Settings of the Processors and Sensor Nodes

Parameters	Value
<b>Switching Capacitance <math>C</math></b>	1.45 nF
<b>Frequency-Voltage Ratio <math>K</math></b>	$0.87 \times 10^9$ MHz/V
<b>Hardware Parameter <math>\varepsilon</math></b>	0.83 V

The derivative of  $E$  with respect to  $\tau_c$  as shown in Equation 57, was negative, which implied that it was always energy-efficient to use longer computation time  $\tau_c$  (lower operating frequency  $f$ ) in processing the task. It also matched the time allocation strategy proposed in the data acquisition scheme.

$$\frac{\partial E}{\partial \tau_c} = - \frac{2N^2 \cdot C}{K \cdot \tau_c^2} \left( \frac{N}{K \cdot \tau_c} + \varepsilon \right) < 0 \tag{57}$$

### 3.3.3.4 Results

Two scenarios were conducted to test the energy efficiency of the proposed reconfigurable data acquisition scheme. In one scheme, sensor nodes utilized DVS technique under the proposed data acquisition scheme. In another scheme, non-reconfigurable sensor nodes used the maximum operating frequency (416MHz) and the

maximum supply voltage (1.25V) to process the task and then transmitted the data with CSMA (Carrier Sense Multiple Access) protocol [52]. The energy for such non-reconfigurable scenario could be expressed as:

$$\begin{aligned}
 E_{non} &= P_{416\text{MHz}} \cdot \tau_c + P_{13\text{MHz}+\text{Radio\_On}} (T - \tau_c) \\
 &= N \cdot C \cdot \left( \frac{f_{416\text{MHz}}}{K} + \varepsilon \right)^2 + P_{13\text{MHz}+\text{Radio\_On}} \left( T - \frac{N}{f_{416\text{MHz}}} \right)
 \end{aligned} \tag{58}$$

Figure 37 shows the captured power consumption variation for the two scenarios.

In the upper diagram of Figure 37, a sensor node with DVS capability first operated at 13MHz (the lowest operating frequency) with radio turning on during the control sub-frame ( $\tau_{control}$ ) to receive the control signals from the CH. Then, the sensor node operated at 286MHz operating frequency with radio off to process the signal processing for  $\tau_c$  and switched back to 13 MHz with radio on to transmit the extracted data for  $\tau_t$ . After the communication task, the sensor node turned off its radio and waited for the next sampling frame. The energy consumption of the sensor node within a sampling frame could thus be measured by summing these time-series power consumption. In the lower diagram of Figure 37, a sensor node without DVS Capability used the maximum operating frequency (416 MHz) in processing the computation task, and then turned the radio on for the remaining sampling frame for data transmission.

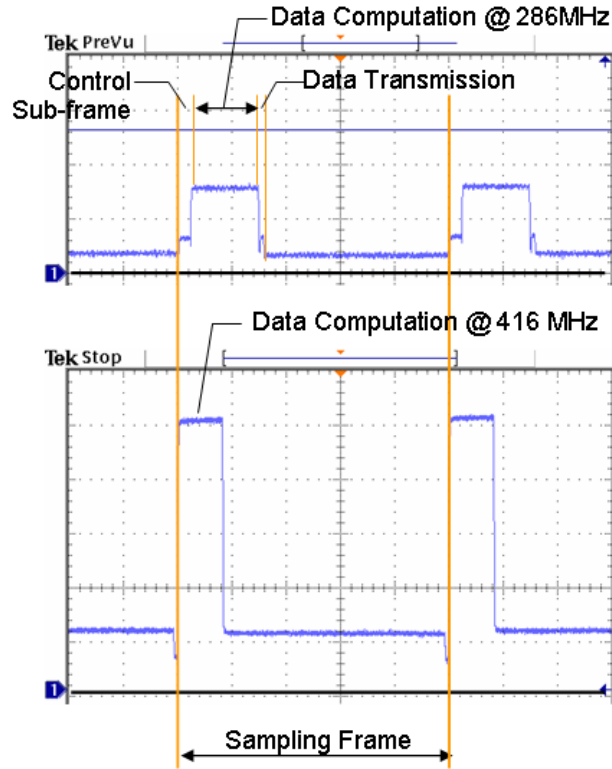


Figure 37: Energy profiling of using reconfiguration and without using reconfiguration technique

Figure 38 illustrates the energy consumption for the two scenarios both from the energy model and from the experimental energy measurement. A slightly difference (< 2.5%) existed between the energy model and the experimental energy measurement, which was primarily due to the non-exactly linear voltage and frequency relation of the processor and discrete operating frequencies available for the sensor nodes.

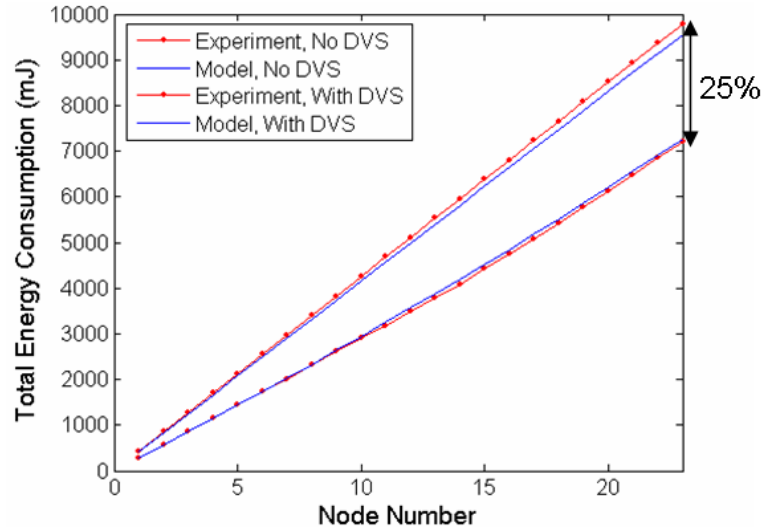


Figure 38: Energy consumption with and without node reconfigurability

The energy model was then used to calculate the energy-efficiency achieved by a reconfigurable sensor network for various length of sampling frame,  $T = 1, 1.5, 2.0, 2.5,$  and 3 seconds. As shown in Figure 39, 20~50% energy saving were achieved of using the DVS technique. The energy-efficiency increased with the increased sampling frame and the decreased number of sensor nodes in a cluster because the available computation time  $\tau_{c,i}$  increased with the prolonged sampling frame and reduced number of sensor nodes in a cluster. The energy reduction partly came from the utilization of previously unallocated time resource to reduce the computation energy; partly energy reduction came from the turn down of the radio after data transmission. In addition, the scheduling of data communication largely reduced the possibility of communication collision, which prevented the loss of data during communication.

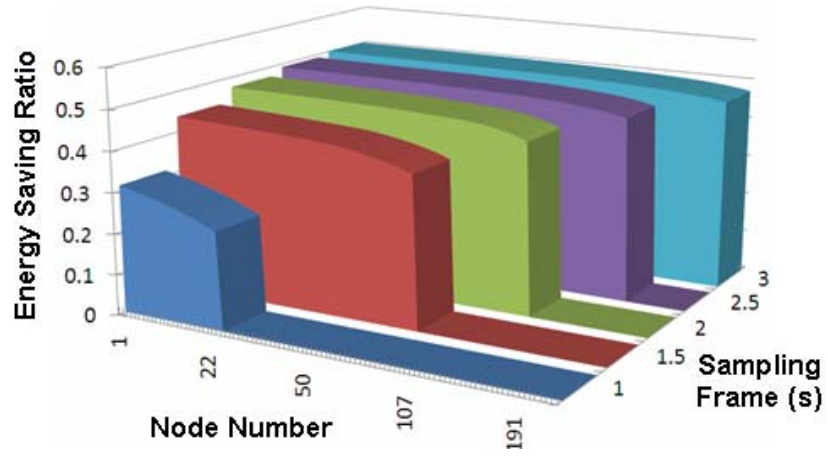


Figure 39: Energy saving for various sampling frame and node number



## CHAPTER 4

### CONCLUSION

This thesis presented a complete framework for the utilization of reconfiguration techniques on the WSN from node-level and network-level. In the node-level reconfiguration, an integration of DVS and DMS techniques was proposed to minimize the total energy consumption within the networks. Applications of data acquisition with real-time constraints were considered. The new scheme achieved energy savings by trading energy against both computation and communication time. The objective was to design a strategy that optimally allocates the limited processing time to computation and communication by adjusting the processor's supply voltage and the radio's modulation level. In order to solve the optimization efficiently, a dynamic time allocation algorithm was developed that utilizes a classification of sensor nodes' energy function and the special structure of the optimization problem to efficiently solve the time allocation problem. The simulation results demonstrated an average 55 percent energy reduction when compared to a node where no energy-aware technique was used. The ineffectiveness of DVS in high communication tasks and high node numbers was also rectified by incorporating DMS into DVS.

In the network-level reconfiguration, an intelligent node activation technique was presented to reduce the cost in recharging energy-depleted sensor nodes in a wireless sensor network. The network operation combined with node activation was modeled as a stochastic decision process, where the activation decisions directly affect the energy efficiency of the network. An analytical model was developed to formulate the network operation as a Semi-Markov Decision Process (SMDP) by assuming exponentially

distributed recharging and discharging times. Using this model, an optimal activation policy was obtained that minimizes the recharging rate. The results of this work are simulated for both a correlated and an independent sensor model. In the correlated sensor model, a 72% reduction of recharging rate has been achieved compared with the scenario where no intelligent node activation was used. The approach presented can be applied to the development of similar types of node activation problems.

A reconfigurable sensor network based on the DVS concept was implemented that enables continued data sampling and on-node data feature extraction. A reservation-based Time Division Multiple Access protocol was employed to allow staggered data transmissions within a sensor cluster. As a result, sensor nodes that were scheduled to transmit their data later in the sequential order can take advantage of the “extra” time allocated to slow down the speed of data processing by lowering the supply voltage, thereby reducing energy consumption. The design of reconfigurable sensor nodes was demonstrated through the integration of a Crossbow Imote2 platform with a customized sensor board. The Imote2 utilized an Intel XScale PXA271 processor with DVS capability. The sensor board, containing a sensor interface and an A/D converter, was designed for high sampling rate applications enabled by Direct Memory Access (DMA) through the Serial Peripheral Interface of the CPU. As a result, concurrent processing of signal sampling and local data computation were achieved for real-time applications. To evaluate the developed data acquisition scheme, a sensor network was designed that features autonomous sensor cluster head selection, time synchronization, and dynamic allocation of computation times at the sensor node level. Its performance was comparatively evaluated against a conventional sensor network that employs maximum

operating frequency for task execution and transmission using the Carrier Sense Multiple Access (CSMA) protocol. Energy models for these two comparative scenarios were first developed, and simulation results were compared experimentally. It was found that energy reduction of up to 50% could be achieved using the reconfigurable sensor hardware, which effectively translates into prolonged service life of the sensor network.

## BIBLIOGRAPHY

- [1] Z. Chaczko and F. Ahmad, "Wireless Sensor Network Based System for Fire Endangered Areas," Proceedings of the third International Conference on Information Technology and Applications (ICITA'05), Sydney, July, 2005.
- [2] A. Mainwaring, J. Polastre, R. Szewczyk, D. Culler, and J. Anderson, "Wireless Sensor Networks for Habitat Monitoring," Proceedings of the 1<sup>st</sup> ACM International Workshop on Wireless Sensor Networks and Applications (WSNA'02), Atlanta, Georgia, USA, September, 2005.
- [3] N. Xu, S. Rangwala, K.K. Chintalapudi, D. Ganesan, A. Broad, R. Govindan, and D. Estrin, "A Wireless Sensor Network For Structural Monitoring," ACM SenSys'04, Baltimore, Maryland, USA, November, 2004.
- [4] Y. Wang, J.P. Lynch, K.H. Law, "Design of a Low-Power Wireless Structural Monitoring System for Collaborative Computational Algorithms," Proceedings of SPIE 12<sup>th</sup> Annual International Symposium on Smart Structures and Materials, San Diego, CA, March, 2005.
- [5] R. Gao, A. Deshmukh, R. Yan, and Z. Fan, "Energy Efficient Wireless Sensor Network for Dynamic System Monitoring", SPIE International Symposium on Intelligent Systems in Design and Manufacturing, Vol. 5999, paper #5999-04, Boston, MA, 2005.
- [6] Arora et al., "A Line in the Sand: A Wireless Sensor Network for Target Detection, Classification, and Tracking," Computer Networks, Vol. 46, Issue 5, pp. 605-634, 2004.
- [7] M. Duarte and Y. Hu, "Vehicle Classification in Distributed Sensor Networks," Journal of Parallel and Distributed Computing, Vol. 64, Issue 7, 2004.
- [8] D. Li, K. Wong, Y. Hu, and A. Sayeed, "Detection, Classification and Tracking of Targets in Distributed Sensor Networks," IEEE Signal Processing Magazine, Vol. 19, Issue 2, pp. 17-29, 2002.
- [9] V. Shnayder, B. Chen, K. Lorincz, T.R.F. Fulford-Jones, and M. Welsh, "Sensor Networks for Medical Care," Technical Report TR-08-05, Division of Engineering and Applied Science, Harvard University, 2005.
- [10] Fuji-Keizai and MRG, Inc., "U.S. Industry & Market Survey: Comprehensive Analysis of Wireless Sensor Systems Market," April, 2006.
- [11] I. Tumer and A. Bajwa, "A Survey of Aircraft Engine Health Monitoring Systems," AIAA/ASME/SAE/ASEE Joint Propulsion Conference and Exhibit, 35th, Los Angeles, CA, June, 1999.

- [12] J. Hill, M. Horton, R. Kling, and L. Krishnamurthy, "The Platforms Enabling Wireless Sensor Network," *Communications of the ACM*, Vol. 47, No. 6, pp. 41-46, June, 2004.
- [13] I. Akyildiz, W. Su, Y. Sankarasubramaniam, and E. Cayirci, "A Survey on Sensor Networks," *IEEE Communications Magazine*, pp. 102-114, August, 2002.
- [14] J. Al-Karaki and A. Kamal, "Routing Techniques in Wireless Sensor Networks: A Survey," *IEEE Wireless Communications*, Vol. 11, Issue 6, pp. 6-28, December, 2004.
- [15] I. Demirkol, C. Ersoy, and F. Alagoz, "MAC Protocols for Wireless Sensor Networks: A Survey," *IEEE Communications Magazine*, Vol. 44, Issue 4, pp. 115-121, April, 2006.
- [16] V. Gutnik and A. Chandrakasan, "Embedded Power Supply for Low-Power DSP," *IEEE Transactions VLSI System*, Vol. 12, pp. 425-435, 1997.
- [17] C. Cassandras and S. Zhuang, "Optimal Dynamic Voltage Scaling for Wireless Sensor Nodes with Real-Time Constraints," *SPIE International Symposium on Intelligent Systems in Design and Manufacturing*, Vol. 5999, paper #5999-02, Boston, MA, 2005.
- [18] P. Pillai and K.G. Shin, "Real-Time Dynamic Voltage Scaling for Low-Power Embedded Operating Systems," *ACM Symposium on Operating Systems Principles*, Alberta, Canada, 2001.
- [19] R. Gao and Z. Fan, "Architectural Design of a Sensory-node-Controller for Optimized Energy Utilization in Sensor Networks", *IEEE Transactions on Instrumentation and Measurement*, Vol. 55, No. 2, pp. 415-428, April 2006.
- [20] C. Schurgers, V. Raganathan, and M. Srivastava, "Power Management for Energy-Aware Communication Systems," *ACM Transactions on Embedded Computing Systems*, Vo. 2, No. 3, pp. 431-447, 2003.
- [21] B. Prabhakar, E.U. Biyikoglu, and A.E. Gamal, "Energy-Efficient Transmission over a Wireless Link via Lazy Packet Scheduling," *Proc. IEEE INFOCOM'2001*, 2001.
- [22] C. Schurgers, O. Aberthorne, and M. Srivastava, "Modulation Scaling for Energy Aware Communications," In *Proceedings ISLPED'01*, Huntington Beach, CA, pp. 96-99, August, 2001.
- [23] Y. Yao and G. Giannakis, "Energy-Efficient Scheduling for Wireless Sensor Networks," *IEEE Transactions on Communications*, Vol. 53, No. 8, 2005.

- [24] E.U. Biyikoglu, B. Prabhakar, and A. Gamal, "Energy-Efficient Packet Transmission Over a Wireless Link," *IEEE/ACM Transactions on Networking*, Vol. 10, No. 4, pp. 487-499, August 2002.
- [25] E.U. Biyikoglu and A. Gamal, "On Adaptive Transmission for Energy Efficiency in Wireless Data Networks," *IEEE Transactions on Information Theory*, Vol. 50, No. 12, pp. 3081-3094, December 2004.
- [26] Y. Yu, B. Krishnamachari, and V.K. Prasanna, "Energy-Latency Tradeoffs for Data Gathering in Wireless Sensor Networks," *IEEE INFOCOM'2004*, 2004.
- [27] Z. Yang, Y. Yuan, J. He, and W. Chen, "Adaptive Modulation Scaling Scheme for Wireless Sensor Networks," *IEICE Transactions on Communications*, Vol. E88-B, No. 3, 2005.
- [28] K. Cho and H. Samuelli, "A 8.75-MBaud Single-Chip Digital QAM Modulator with Frequency-Agility and Beamforming Diversity," *Proceedings of the IEEE 2000 Custom Integrated Circuits Conference*, Orlando, FL, pp. 27-30, May, 2000.
- [29] Y. Wu and Y. Shayan, "Implementation of High-Speed Multi-Level QAM Modems Based on Xilinx Virtex-II FPGA," *IEEE Canadian Conference on Electrical and Computer Engineering (CCECE)*, Montreal, May, 2003.
- [30] C. Yeh, Z. Fan, and R. Gao, "Energy-Aware Data Acquisition in Wireless Sensor Networks," *Proceedings of the IEEE Instrumentation and Measurement Technology Conference (IMTC)*, Warsaw, Poland, May, 2007.
- [31] Intel Inc., "Intel PXA27x Processor Family Electrical, Mechanical, and Thermal Specification," [www.intel.com](http://www.intel.com), 2005.
- [32] T. Ue, S. Sampei, N. Morinaga, and K. Hamaguchi, "Symbol Rate and Modulation Level-Controlled Adaptive Modulation/TDMA/TDD System for High-Bit Rate Wireless Data Transmission," *Trans. on Vehicular Technology*, Vol. 47, No. 4, pp. 1134-1147, Nov. 1998.
- [33] J. Proakis, "Digital Communications," *McGraw-Hill Series in Electrical and Computer Engineering*, McGraw-Hill New York, 1995.
- [34] W.R. Heinzelman, A. Chandrakasan, and H. Balakrishnan, "Energy-Efficient Communication Protocol for Wireless Microsensor Networks," *Proceedings of International Conference on System Sciences*, 2000.
- [35] D. Goodman, R. Valenzuela, K. Gayliard, and B. Ramamurthi, "Packet Reservation Multiple Access for Local Wireless Communication," *IEEE Transactions on Communications*, Vol. 37, No. 8, pp. 885-890, 1989.

- [36] W. Heinzelman, A. Chandrakasan, and H. Balakrishnan, "An Application Specific Protocol Architecture for Wireless Microsensor Networks," *IEEE Transactions on Wireless Networking*, 2002.
- [37] C. Liu, K. Wu, Y. Xiao, and B. Sun, "Random Coverage with Guaranteed Connectivity: Joint Scheduling for Wireless Sensor Networks," *IEEE Transactions on Parallel and Distributed Systems*, Vol. 17, Issue 6, pp. 562-575, 2006.
- [38] S. Meguerdichian, F. Koushanfar, M. Potkonjak, and M. B. Srivastava, "Coverage Problems in Wireless Ad-hoc Sensor Networks," *Proceedings IEEE Infocom*, pp. 1380-1387, 2001.
- [39] B. Liu and D. Towsley, "A Study of the Coverage of Large-scale Sensor Networks," *IEEE International Conference on Mobile Ad-hoc and Sensor Systems*, Fort Lauderdale, Florida, USA, October, 2004.
- [40] A. LaMarca et al., "Making Sensor Networks Practical with Robots," *International Conference on Pervasive Computing*, Zurich, Switzerland, August, 2002.
- [41] M. Rahimi, H. Shah, G. Sukhatme, J. Heideman, and D. Estrin, "Studying the Feasibility of Energy Harvesting in a Mobile Sensor Network," *Proceedings of the 2003 IEEE International Conference on Robotics & Automation*, Taipei, Taiwan, September, 2003.
- [42] A. Kansal, M. Rahimi, D. Estrin, W. Kaiser, G. Pottie, and M. Srivastava, "Controlled Mobility for Sustainable Wireless Sensor Networks," *IEEE Communications Society Conference on Sensor and Ad Hoc Communications and Networks*, 2004.
- [43] K. Kar, A. Krishnamurthy, and N. Jaggi, "Dynamic Node Activation in Networks of Rechargeable Sensors," *IEEE/ACM Transactions on Networking*, Vol. 14, No. 1, pp. 15-26, 2006.
- [44] T. Banerjee and A. Kherani, "Optimal Control of Admission to a Station in a Closed Two Queue System," *Proceedings of the First International Conference on Performance Evaluation Methodologies and Tools (Valuetools)*, Pisa, Italy, October, 2006.
- [45] M. Schal, "Average Optimality in Dynamic Programming with General State Space," *Mathematics of Operations Research*, Vol. 18(1), 1993.
- [46] R. Bellman, "Dynamic Programming," Princeton, N.J.: Princeton University Press, 1957.
- [47] R. Bellman, "Adaptive Control Processes: A Guided Tour," Princeton, N.J.: Princeton University Press, 1961.

- [48] A. Gosavi, "Simulation-Based Optimization: Parametric Optimization Techniques & Reinforcement Learning," Kluwer Academic Press, 2003.
- [49] A. Arora et al., "ExScal: Elements of an Extreme Scale Wireless Sensor Network," Proceedings of the 11<sup>th</sup> IEEE International Conference on Embedded and Real-Time Computing Systems and Applications (RTCSA'05), Vol. 00, pp. 102-108, 2005.
- [50] M. Maroti, B. Kusy, G. Simon, and A. Ledeczi, "The Flooding Time Synchronization Protocol," Technical Report TR#ISIS-04-501, Institute for Software Integrated Systems, Vanderbilt University, 2004.
- [51] R. Yan and R. Gao, "An Efficient Approach to Machine Health Evaluation Based on Harmonic Wavelet Packet Transform," Robotics and Computer Integrated Manufacturing, Vol. 21, pp. 291-301, 2005.
- [52] A. Woo and D. Culler, "A Transmission Control Scheme for Media Access in Sensor Networks," Proceedings of the 7<sup>th</sup> annual international conference on Mobile computing and networking, pp. 221-235, Rome, Italy, 2001.